PET respiratory motion correction: quo vadis?

Frederic Lamare, A. Bousse, K. Thielemans, C. Liu, T. Merlin, H. Fayad, D. Visvikis

▶ **To cite this version:**

Frederic Lamare, A. Bousse, K. Thielemans, C. Liu, T. Merlin, et al.. PET respiratory motion correction: quo vadis?. Physics in Medicine and Biology, 2022, 67 (3), 10.1088/1361-6560/ac43fc . hal-04090024

HAL Id: hal-04090024
https://hal.science/hal-04090024

Submitted on 5 May 2023

HAL is a multi-disciplinary open access archive for the deposit and dissemination of scientific research documents, whether they are published or not. The documents may come from teaching and research institutions in France or abroad, or from public or private research centers.

L'archive ouverte pluridisciplinaire **HAL**, est destinée au dépôt et à la diffusion de documents scientifiques de niveau recherche, publiés ou non, émanant des établissements d'enseignement et de recherche français ou étrangers, des laboratoires publics ou privés.

PET Respiratory Motion Correction: Quo Vadis?

F. Lamare[1,2], A. Bousse[3], K. Thielemans[4], C. Liu[5], T. Merlin[3], H. Fayad[6], D. Visvikis[3]

[1] Nuclear Medicine Department, University Hospital of Bordeaux, Bordeaux, F-33000, France

[2] University of Bordeaux, CNRS, EPHE, INCIA, UMR 5287, Bordeaux, F-33000, France

[3] LaTIM, INSERM UMR 1101, Université de Bretagne Occidentale, 29238 Brest, France

[4] Institute of Nuclear Medicine, University College London, London, UK

[5] Department of Radiology and Biomedical Imaging, Yale University, New Haven, USA

[6] Weill Cornell Medicine-Qatar, Doha, Qatar

E-mail: `frederic.lamare@chu-bordeaux.fr`

January 2021

Abstract. Positron emission tomography (PET) respiratory motion correction has been a subject of great interest for the last twenty years, prompted mainly by the development of multimodality imaging devices such as PET/computed tomography (CT) and PET/magnetic resonance imaging (MRI). PET respiratory motion correction involves a number of steps including acquisition synchronization, motion estimation and finally motion correction. The synchronization steps include the use of different external device systems or data driven approaches which have been gaining ground over the last few years. Patient specific or generic motion models using the respiratory synchronized datasets can be subsequently derived and used for correction either in the image space or within the image reconstruction process. Similar overall approaches can be considered and have been proposed for both PET/CT and PET/MRI devices. Certain variations in the case of PET/MRI include the use of MRI specific sequences for the registration of respiratory motion information. The proposed review includes a comprehensive coverage of all these areas of development in field of PET respiratory motion for different multimodality imaging devices and approaches in terms of synchronization, estimation and subsequent motion correction. Finally, a section on perspectives including the potential clinical usage of these approaches is included.

Nomenclature

1-D one-dimensional

2-D two-dimensional

3-D three-dimensional

4-D four-dimensional

[^{18}F]FDG [^{18}F]fluorodeoxyglucose

AC attenuation-corrected

ACF attenuation correction factor

APD avalanche photo diode

CFR coronary flow reserve

CMRA coronary magnetic resonance angiography

CNN convolutional neural network

COD centroid of distribution

COM center of mass

CT computed tomography

DD data-driven

DR dimensionality reduction

ECG electrocardiogram

EM expectation-maximization

FBP filtered backprojection

FT Fourier transform

HM histogram-mode

IDIF image derived input function

JRM joint reconstruction and motion estimation

LE Laplacian eigenmaps

LM list-mode

LOR line of response

MBIR model-based image reconstruction

MCBR motion correction before reconstruction

MCIR motion-corrected image reconstruction

MIP maximum intensity projection

MLAA maximum-likelihood attenuation and activity estimation

MLACF maximum-likelihood activity and attenuation correction factors estimation

MR magnetic resonance

MRI magnetic resonance imaging

NAC non-attenuation-corrected

PC principal component

PCA principal component analysis

PET positron emission tomography

PRR post-reconstruction registration

PSF point spread function

ROI region of interest

RPM real-time position management

SAM spectral analysis method

SiPM silicon photomultipliers

SNR signal-to-noise ratio

SPECT single-photon emission computed tomography

SUV standardized uptake value

TAC time-activity curve

TMRI tagged magnetic resonance imaging

TOF time-of-flight

1. Introduction

PET imaging has seen important technical progress during the last decades, both in hardware (scintillation crystals, photomultipliers, avalanche photo diodes (APDs), silicon photomultipliers (SiPM), analog and digital signal processing electronics) and software (scatter correction algorithms, image reconstruction algorithms, etc.). Newly commercialized PET/CT systems offer a combination of improved spatial and temporal resolution, a better accuracy in terms of measured radiotracer concentrations, associated with reduced acquisition times and/or reduced injected dose to the patient.

In parallel to these technical advances, patient motion has been demonstrated as one of the most prevalent cause of image artifact in PET (Beyer et al. 2003, Osman et al. 2003, Hunter et al. 2016). Based on phantom acquisitions and simulated results, Liu et al. (2009) observed a 28% reduction in standardized uptake value (SUV) and a 130% increase in volume due to motion. PET is a quantitative imaging modality by nature, offering the possibility to quantitatively assess the tracer concentrations, both in static investigations with the SUVs, and also in dynamic studies aiming at quantifying the tracer transport constants through the use of a kinetic model. Not accounting for subject motion can lead to a potentially severe image quality degradation and a reduced quantitative accuracy. The motion-induced artifacts, in turn, can lead to misinterpretation of images and cause errors in subsequent image analysis or in image-derived information such as PET tumoral volume derived from SUV-based thresholding, which can be used for subsequent radiotherapy treatment planning, especially for focal radiation therapy with dose escalation.

Many techniques for the correction of motion corrupted PET images have been developed in parallel to the technical advances of PET/CT systems during the last 20 years. And yet the complexities of dynamic human anatomy, and the desire to improve the trade-off between image quality, patient dose and scan time, mean that

three decades later motion correction remains a topic of investigation. The developed motion compensation strategies have not as such found widespread acceptance in clinical practice, mainly due to the complexity of their implementation and the associated computational burden.

Related reviews have been made on motion correction in PET. Visvikis et al. (2006) covered the importance of motion compensation in PET/CT systems and contrasted the correction techniques now often referred to as post-reconstruction registration (PRR) and motion-corrected image reconstruction (MCIR). Rahmim et al. (2007) offer a comprehensive review, covering motion measurement and acquisitions, temporal modeling techniques considering a range of anatomical regions. Nehmeh & Erdi (2008) provide a review of motion correction for PET, CT, and PET/CT, covering a range of acquisition and temporal modeling techniques, and focusing on motion artifacts introduced during attenuation correction. Bettinardi et al. (2010) and (Bettinardi et al. 2012) review motion management for PET/CT for radiotherapy planning. McClelland et al. (2013) present a review on respiratory motion models, and include some applications for PET/magnetic resonance (MR) motion correction. More recently, Gillman et al. (2017) wrote a review on PET motion correction dedicated to PET/MR. A recent book chapter presented a general overview of any type of motion compensation strategy for single photon or positron emission tomography (van den Hoff et al. 2020). In addition, Kyme & Fulton (2021) review motion estimation and correction methods in PET, single-photon emission computed tomography (SPECT) and CT. Finally, Polycarpou et al. (2021) provides an up-to-date review on the synergistic use of both PET and MR data for PET motion correction in simultaneous PET/MR.

The purpose of this review is to present the range of published methods developed to address the issue of respiratory motion compensation in PET imaging. The detection or estimation of the respiration signal will be addressed, as well as the management of the motion information within the context of PET image reconstruction.

2. Respiratory Motion Management

Methodologies for respiratory motion correction in PET can be decomposed into four successive stages: acquisition, gating, motion estimation and correction.

Acquisition involves the simultaneous acquisitions of the PET raw data (detected events) and the patient respiratory signal (Figure 1). The respiratory signal may be recorded using an external device for the entire PET acquisition duration (see Section 3.1) or derived from the raw PET data themselves (see Section 3.2). PET acquisitions are preferably acquired in list-mode (LM) format, or at least in discrete temporal sinograms. The LM format offers the advantage of a high temporal resolution, with specific time marks inserted within the raw PET detected events every 100 ms or so. Moreover, when using an external device to track the patient respiration, the external device also synchronizes the recorded continuous respiratory signal with the PET LM acquisition using a simple trigger method. Once the recorded respiratory trace reaches

a predefined threshold value, a specific trigger is inserted into the LM PET data to mark this specific instant of the respiratory cycle. The process is repeated at each respiratory cycle, i.e., each time the trigger threshold is reached. When the surrogate signal for the respiratory motion is directly extracted from the PET measured data, PET acquisition and derived respiratory signal are intrinsically synchronized. Such an approach facilitates the identification of irregular respiratory cycles, either in amplitude or in duration, and the rejection of the corresponding raw emission data.

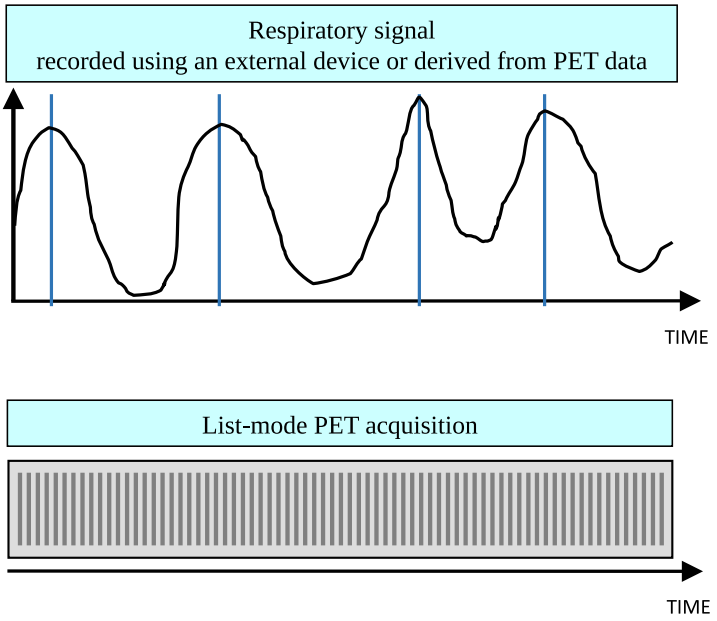

Figure 1: Simultaneous acquisitions of the PET raw data in LM format and the patient respiratory signal, either recorded using an external tracking system, or directly derived from the PET data.

The gating process consists in the division of the respiratory motion signal into a number of possible respiratory states. With an appropriate combination of the number of states (usually between 6 and 10), and the division method, only a small amount of respiratory motion (ideally negligible) remains present within each respiratory state. Different division methods have been proposed (see Section 3.3). With the synchronization of the PET acquisition and the continuous respiratory signal previously described, the gating process not only consists in dividing the respiratory signal in different states, but most importantly aims at labeling each PET detected event with the corresponding respiratory state, by reading in parallel the respiratory signal and the synchronized PET LM file (Figure 2). It becomes therefore possible to reconstruct a PET images series synchronized with respiration, each gated PET image corresponding to one respiratory state. It is evident that the resulting respiration-synchronized images are less influenced by breathing, but are still not entirely free from these effects. The second problem encountered is that the different reconstructed synchronized images are of reduced quality, essentially because they only contain a fraction of the total number

of events detected during the PET acquisition (Visvikis et al. 2006). As a result, the benefits of motion compensation can be significantly reduced, as lower statistics in images can reduce the accuracy of the activity concentration measurement, as well as functional volume size. These detrimental effects can be compensated for, however, by increasing the acquisition time by a factor equivalent to the number of reconstructed synchronized images.

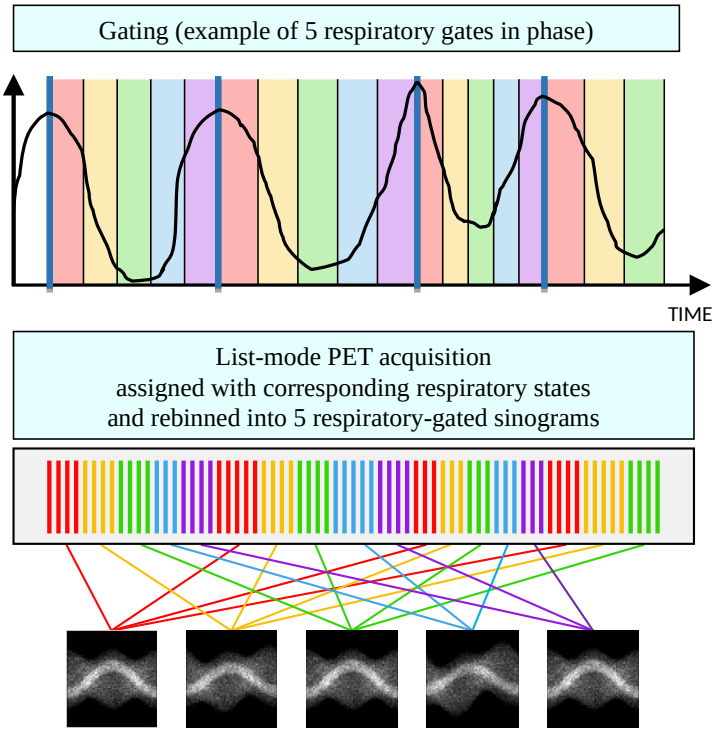

Figure 2: Gating process: division of the respiratory signal in different respiratory states, and labeling of each PET detected event with the corresponding respiratory state

To overcome these limitations, respiratory motion compensation methods have been developed, involving the determination of the respiratory motion, and its subsequent implementation to the PET data.

Respiratory model formation estimates appropriate model parameters to correct the PET acquisition for breathing (see Section 4). The chosen model can be a rigid, affine or non-affine, the latter often parametrized in terms of B-spline warp parameters, to move the current respiratory bin back to the reference state, or can be a simple binary signal representing in-phase or out-of-phase (Figure 3). For respiratory motion, the reference state is often selected as end-exhale because this is the quiescent part of the respiratory cycle.

Finally, the correction phase appropriately applies the respiratory motion parameters derived from the registration of the respiratory gated PET image series. Motion correction may be performed before reconstruction, during reconstruction (on the system matrix), or after reconstruction, as described in Sections 5.2, 5.3 and 5.4.

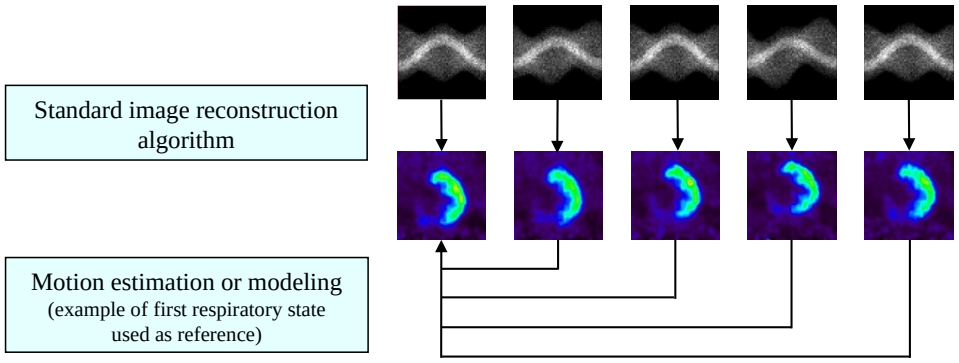

Figure 3: Motion modeling and estimation

3. Motion Synchronization and Detection

In order to synchronize the PET acquisition with the respiration, it is necessary to ensure that the respiratory signal covering the entire duration of the PET acquisition is available. The respiratory trace of the patient can either be recorded using an external device tracking the patient respiration (Section 3.1), or be directly derived from the PET raw data (Section 3.2). Section 3.3 describes how the PET data can be gated into different respiratory states based on the synchronous respiratory trace.

3.1. Motion Tracking Systems

This section describes the available technologies for tracking the patient respiratory signal in PET, which can be grouped into two main categories. The first is based on the use of an external detection system in contact with the patient's body: a sensor measuring the impedance of a belt placed around the rib cage which varies according to its elongation (Livieratos et al. 2005a, van Elmpt et al. 2011), or respiratory bellows (Lang et al. 2006), a thermistor measuring the temperature of the air circulating during the patient's breathing (Boucher et al. 2004, Wolthaus et al. 2005), a spirometer measuring inhaled and exhaled air flows, measurements of air flux, for example endotracheally (Chun, Reese, Ouyang, Guérin, Catana, Zhu, Alpert & El Fakhri 2012) (this method is often used in animal studies, but rarely in human studies due to its invasive nature). Optical motion tracking methods perform a quantitative measure of external motion due to respiration, providing an accurate surrogate. For example, by attaching fiducials to the patient's chest, one-dimensional (1-D) chest movement can be measured (Abdelnour et al. 2007, Büther et al. 2009, Dawood et al. 2007, Huang et al. 2014, Nehmeh et al. 2002, Nehmeh et al. 2003, Nehmeh, Erdi, Pan, Yorke, Mageras, Rosenzweig, Schoder, Mostafavi, Squire, Pevsner, Larson & Humm 2004, Nehmeh, Erdi, Pan, Pevsner, Rosenzweig, Yorke, Mageras, Schoder, Vernon, Squire, Mostafavi, Larson & Humm 2004). Such external devices are reliable, relatively cheap, and easy to use, but they often measure a process indirectly related with respiration, such as air flow rate, causing a time shift between the respiration related organs motion, and the device

measurement, which is problematic for the synchronisation of the PET acquisition with respiration.

In the second category, contact-less external systems track the patient's body contours and surface from a distance. Advanced methods are based on the use of stereoscopic or time-of-flight (TOF) cameras (Alnowami et al. 2012, Gilles et al. 2016, Kyme et al. 2014, Heß et al. 2015), or high-precision systems such as laser scanners which derive surface models of the monitored object without the need for fiducials (Brahme et al. 2008). Although optical devices require additional hardware and processing, they remain relatively simple to implement.

A possible limitation of all external tracking systems is the additional hardware setup, which may be uncomfortable for the patient, and require additional time for the patient preparation, especially for patients with psychological (Törnqvist et al. 2006) or neurological (González et al. 1999) conditions, or in pediatrics (Edwards & Arthurs 2011).

Bettinardi et al. (2013) have published an extensive review about motion-tracking systems, including respiratory motion tracking systems, and their applications in PET/CT imaging.

3.2. PET Data-Driven Methodologies

There is an increasing interest in methods that extract a surrogate signal for the respiratory motion directly from the PET measured data (Kesner et al. 2014), often called "data-driven" or "device-less" gating or also "self-gating". This is motivated by the extra cost and patient management associated to the additional device, potential issues due to the capability of the external device (Lupi et al. 2009, Liu et al. 2010, Didierlaurent et al. 2012), but also because of some evidence of hysteresis between the internal movement and external device (Ozhasoglu & Murphy 2002, Gierga et al. 2005). In the following few paragraphs, we review this work concentrating on methods that have been applied to PET data.

3.2.1. Image-Based Methods Initial work used the sequence of images reconstructed without attenuation, obtained for instance every 0.5 s. Many groups compute the center of mass (COM) in an region of interest (ROI) and use this as an indicator of motion (Klein et al. 2001, Bundschuh et al. 2007) and cardiac SPECT (Bruyant et al. 2002). Filtering allows separation of a respiratory and cardiac signal in cardiac PET (Büther et al. 2009). Visvikis et al. (2003) placed an ROI over edges of boundaries (using non-attenuation corrected images) and studied the time-activity curve (TAC). A characteristic frequency was derived via the Fourier transform (FT) which then allowed finding amplitude and phase images. Blume et al. (2012) used cross-correlation between low-resolution images reconstructed from 1 s time frames and optimized a cost-function to maximize the cross-correlation between time frames in each gate. These image-based methods are however computationally expensive and need a high contrast region, such

as the myocardium in cardiac studies, that can be tracked over time.

3.2.2. Sinogram-Based Methods More recently, many authors developed methods that work on the projection data. Although the PET raw data are very large, most methods were developed for down-sampled data such that memory requirements are drastically reduced. Schleyer et al. (2009) then Schleyer et al. (2011) used an analysis in frequency space to attempt to find dominant respiratory frequencies but proceeds by automatically finding masks where the movement occurs. A novel idea in this method was to convert the mask to a signed template such that edges moving in and out of the mask do not cancel each other. This spectral analysis method (SAM) method was later extended for dynamic PET by using a sliding-window technique. It was tested for cardiac studies (Schleyer et al. 2014). A further extension for continuous bed movement showed good results in first evaluations (Schleyer et al. 2018, Büther et al. 2020). This method forms the basis for the Siemens OncoFreeze AI™ method. Kesner & Kuntner (2010) classified elements of (down-sampled) projection data based on the relative power in a respiratory frequency band, and used this to iteratively construct a TAC of increasing power in the respiratory band.

The previous methods were designed for quasi-periodic movement. A different class of methods applies the generic techniques of dimensionality reduction (DR), also known as "Manifold Learning". DR techniques attempt to find a mapping between a low-dimensional space and the original data such that the structure in the original data can be more easily observed in the low-dimensional space (Van der Maaten et al. 2009). To our knowledge, DR was first used in the context of respiratory and cardiac motion by Zhang et al. (2006) where Isomap (Tenenbaum et al. 2000) was used to map a dynamic sequences of MR images to a two-dimensional (2-D) space, roughly corresponding to respiratory and cardiac movement. Laplacian eigenmaps (LE) (Belkin & Niyogi 2003), a different DR technique, was used for respiratory gating of ultrasound and MRI data (Wachinger et al. 2011). Thielemans, Rathore, Engbrant & Razifar (2011) applied principal component analysis (PCA) (Pearson 1901) for respiratory gating of PET data and four-dimensional (4-D) CT Data. The method selects the principal component with the highest power in the respiratory frequency band. This method forms the basis for the GE MOTIONFREE™ option and has been evaluated on large clinical data-sets (Walker et al. 2019, Liberini et al. 2021).

Advantages of the DR methods include noise-suppression, automatic inclusion of TOF (Bertolli et al. 2016), the fact that they do not rely on detection motion, but can also pick up density changes (Bertolli, Cuplov, Arridge, Stearns, Wollenweber, Hutton & Thielemans 2017), and that they can readily be generalized for other types of motion, including non-periodic motion (see Section 6.3). However, the latter is also a weakness as they can pick up the wrong signal such as kinetics or gross patient motion.

3.2.3. List-Mode-Based Methods The final class of methods works directly from the LM data, without constructing intermediate dynamic sinograms.

A method for respiratory gating specific to three-dimensional (3-D) PET (and which does not need any ROIs) was developed by He et al. (2008). The approach relies on the fact that axial motion will affect the total count rate, due to the axially non-uniform sensitivity in 3-D PET. The count rate is therefore used as the respiratory signal.The main advantage of this method is that it is very easy to implement. It can in principle also give information about non-periodic movement. However, it relies on axial motion and sufficient contrast.

The COM method can be implemented directly on the LM data, called centroid of distribution (COD) by some authors. This benefits from the availability of TOF as it allows concentrating on a ROI (Ren et al. 2017). Feng et al. (2017) developed a method that optimised the ROI to get a better respiratory signal.

3.2.4. Sign and Scale Determination All of the above methods obtain a signal that suffers from ambiguity in both scale and sign. This is even the case for the COM method, see (Feng et al. 2017).

The sign ambiguity can be particularly detrimental in whole-body studies as it could lead to amalgamation of end-of-inspiration and end-of-expiration data in the same gate. Schleyer et al. (2011) estimate the sign from (rigid) registration of maximum intensity projection (MIP) images reconstructed with filtered backprojection (FBP) (without attenuation correction). Bertolli, Arridge, Wollenweber, Stearns, Hutton & Thielemans (2017) developed two sinogram methods based on the approximation that the motion is in axial direction only, and investigating the correlation between the data-driven (DD) signal/principal component (PC) obtained from this approximation and actual data-driven result. Feng et al. (2017) tested a simple method that detects asymmetry in the DD signal. While the former methods aim to assign expiration and inspiration correctly, the latter aims only for consistency between the different bed positions, which is sufficient in nearly all cases.

For many applications, the scale of the signal can remain arbitrary, for instance when phase gating is used. Even for displacement gating, the scale is irrelevant as long as it remains constant over time. This is however not the case when comparing the signals of different bed positions or when tracer kinetics are present. COM is less sensitive to the latter, although still influenced by contrast changes (Feng et al. 2020). Current methods to stabilize the scale include base-line correction with low-order polynomials or splines (Bertolli, Arridge, Wollenweber, Stearns, Hutton & Thielemans 2017, Schleyer et al. 2018), amplitude-normalization over long time scales (Schleyer et al. 2018) and band-pass filters (Feng et al. 2020). This methods are somewhat *ad hoc*, see Section 3.3 for further discussion.

3.2.5. Comparison Studies All cited papers compare the DD signal with a hardware tracker, or sometimes MR navigator, usually reporting correlation coefficients. However, only a few papers have compared different DD methods against each other (Thielemans et al. 2013, Ren et al. 2019). Such comparisons are not easy as even the hardware signal

can be sub-optimal. Bertolli (2018) developed a metric for intra-gate movement to compare methods, while Ren et al. (2019) used contrast in motion-corrected images. However, in clinical practice, such comparisons between methods are possibly of lesser interest nowadays as the state-of-the-art DD methods perform at least as well the hardware methods (Büther et al. 2020, Walker et al. 2019, Liberini et al. 2021).

3.3. Gating Methodologies

With either external motion tracking system or data-driven approaches, a respiratory signal over time can be obtained and synchronized with PET LM data. Subsequently, various gating methods can be applied to generate respiratory gates to reduce motion and facilitate motion vectors estimation for advanced motion correction as described in Section 5. The most commonly used gating methods are phase gating and amplitude gating (Kitamura et al. 2017) (Figure 4). In phase gating, LM data within each respiratory cycle is divided into several equal phase gates, and corresponding gates across cycles are combined to generate each phase gated image. Five to eight phase gates are typically used in clinical studies. In amplitude gating, LM data with the same displacement range is grouped together regardless of cycle and phase information. Amplitude gating can be further categorized into equal counts and equal amplitude gating (Jani et al. 2013). In "equal counts" gating, all gates contain the same amount of detected events, leading to the same image noise across gated images. However, as patients could spend more time during expiration than inspiration, such expiration gates tend to contain less intra-gate motion while inspiration gates contain larger amounts of intra-gate motion, leading to more blurred gated images. To address this gate-dependent blurring issue, "equal amplitude" gating was proposed to keep the amount of intra-gate motion the same across gates by grouping LM events within the same displacement range. However, this strategy results in different counts/noise levels across gates, which could lead to gate-dependent quantification variability and pose registration challenges for motion estimation (Section 4). In some applications, gating is performed on both displacement and its time-derivative (or phase), see Table 7 in (McClelland et al. 2013) for references. However, due to the high noise level in the resulting gates, this is generally only used in combination with motion correction techniques (see Section 5). As opposed to generating many low count gates, since most patients spend more time breathing at expiration, LM data only from the end-expiration gate, either defined by phase or displacement, can be used to generate a single gated image (Liu et al. 2010, van Elmpt et al. 2011), now available as commercial products GE Q.Static™ and Siemens HD-Chest™. Such image with better trade-off between image noise and intra-gate motion can contain 30-50% counts with minimal intra-gate motion.

When the respiratory pattern is regular with consistent baseline and amplitude, phase gating and amplitude gating as well as end-expiration gating can all provide satisfactory gated images with minimal intra-gate motion. However, with significant motion pattern change (Liu et al. 2009), all gating method encounter challenges.

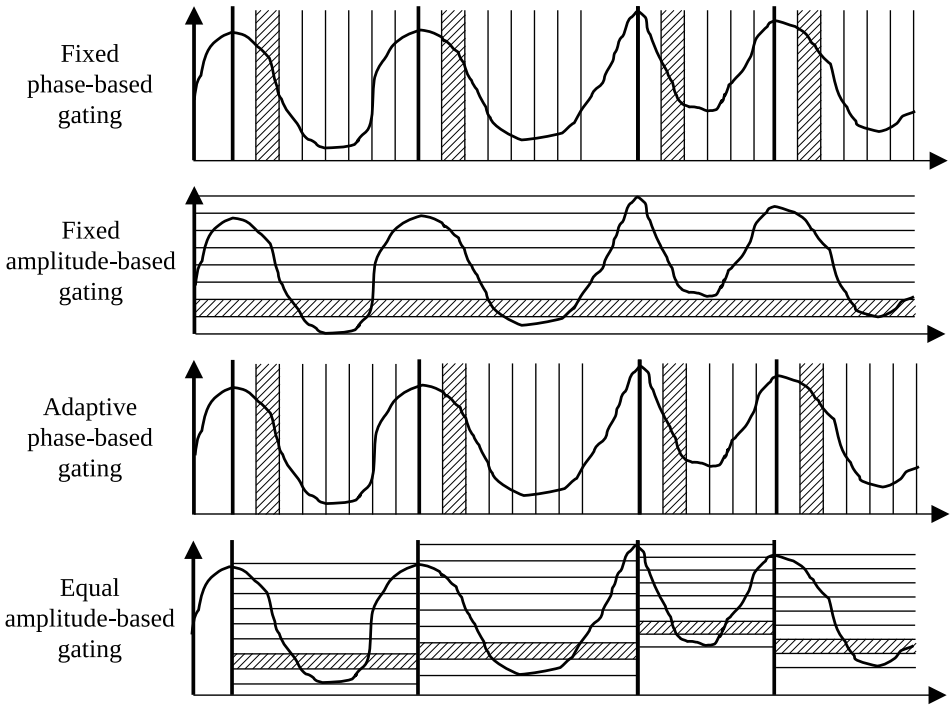

Figure 4: Different gating methodologies, involving a division of the respiratory signal in either phase or amplitude, with a bin length either defined by phase or displacement. The bin length can be fixed, based on an average value computed over the whole acquisition or adapted to each respiratory cycle.

Both intra-cycle variation and inter-cycle variation contribute to intra-gate motion. Larger motion amplitudes within cycles increase intra-cycle variation, while long-term amplitude variation and baseline change contribute to inter-cycle variation (Chan et al. 2013). When long-term amplitude variation and baseline change is observed, one might attempt to normalize amplitude and/or correct baseline of the respiratory signal first prior to gating. Such corrections are controversial. If a patient's internal organ movement correlates well with the motion signal, either by external device or data-driven approaches, corrections of baseline and amplitude will cause errors and additional image blurring in gated images as internal-external correlations are disrupted. On the other hand, when patients' internal organ movement does not correlate with motion signals, such as muscle relaxation induced baseline shift, correction of baseline and amplitude is expected to improve the quality of gated images. The optimal choices in such situations are likely patient specific (Gaede et al. 2009, Ionascu et al. 2007, Beddar et al. 2007). Therefore, advanced data-driven gating guided by motion information derived directly from internal organs might have advantages, while external devices with high temporal resolution also have unique advantages. Combination of data-driven and device-driven gating could be a promising direction to address challenges of respiratory pattern change.

4. Motion Estimation and Modeling

As previously discussed, respiratory gating produces gates that have low signal-to-noise ratio (SNR) since each of the PET gates contains reduced statistics; these synchronized PET gates (4-D PET) can be used for motion estimation. Alternatively, respiratory-synchronized CT images (4-D CT or 4-D MR) can also be used. This is most commonly done by image registration of the gated images (Section 4.1). However, this can lead to limited temporal resolution of the correction process, which depends directly on the number of produced dynamic volumes. In order to resolve such issues, motion modeling is a potential solution (Section 4.2). These models provide continuous information about the internal patient motion based on some surrogate.

4.1. Motion Estimation Using Registration

For several years, respiratory-gated CT seemed to be the only accurate way to accurately pre-estimate a respiratory motion field. Using a "cine" protocol (Pan et al. 2004) synchronized with the PET, it is possible to derive a sequence of high-resolution CT synchronized with the respiratory-gated PET, such that the estimated motion obtained from the registration of the CT images can be used for MCIR (Section 5.3) (Manjeshwar et al. 2006, Qiao et al. 2006, Li et al. 2006, Lamare, Carbayo, Cresson, Kontaxakis, Santos, Cheze-Le Rest, Reader & Visvikis 2007). However, respiratory-gated 4-D CT involves much higher radiation dose and is not feasible in diagnostic PET imaging. In addition, breathing pattern changes between PET and 4-D CT could introduce motion vector mismatch.

In absence of gated CT for attenuation correction, Dawood et al. (2008) then Fayad et al. (2013) proposed to pre-estimate the motion from gated non-attenuation-corrected (NAC) reconstructed PET images. This approach has the advantage of requiring a simple setup (gated PET for motion, conventional CT—or MRI—for attenuation), but the motion estimation suffers from the poor contrast of the NAC single-gate reconstructed PET images. GE's Q.Freeze™ (first version: Wollenweber et al. (2012); second version: Thiruvenkadam et al. (2015)) therefore registers the attenuation-corrected (AC) images, ideally reconstructed with matched respiratory-gated CT to avoid issues with attenuation mismatch. See Section 5.7 for methods to overcome this issue.

PET/MR hybrid systems have opened new possibilities for motion correction in PET. By simultaneously acquiring PET and MR, it is possible to derive a 4-D motion field from the high spatial resolution and high-contrast 4-D MRI, without additional radiation exposure. This motion field can be utilized for MCIR (cf. Section 5.3), either on histogram-mode (HM) data (Tsoumpas et al. 2010, Grimm et al. 2013, Petibon et al. 2014, Manber et al. 2015, Manber et al. 2016, Manber et al. 2018), with Grimm et al. (2013) forming the basis for Siemens BodyCompass™, or LM data (Guérin et al. 2011, Chun & Fessler 2012, Fayad, Schmidt, Würslin & Visvikis 2015, Fayad, Odille, Schmidt, Würslin, Küstner, Felblinger & Visvikis 2015, Küstner et al. 2017). It

has been shown to be advantageous to estimate the respiratory motion from both PET and MRI data using a joint cost-function (Fieseler et al. 2014, Kolbitsch et al. 2018).

4.2. Motion Modeling

Motion models encode a relation between the internal deformation and another measurement ("surrogate") that can be obtained at high temporal sampling. Different surrogates have been used, such as the respiratory phase, the value of a respiratory signal (sometimes completed by its time derivative), or even 2-D MR navigators. Motion models are used when it is not possible/practical to directly measure (or estimate) the actual motion of interest with sufficient temporal resolution during image acquisition (Küstner et al. 2019, McClelland et al. 2013). Considering a 5 s mean respiratory cycle, this temporal resolution is usually fixed to 833 ms in case six temporal frames are used and in the best case to 500 ms for 10 used frames. Moreover, while motion estimation from gated images assumes that respiratory motion is the same from cycle to cycle (for phase gating) or the value of the respiratory signal (for amplitude gating), motion models try to model the inter cycle (breathing difference from cycle to cycle) and intra-cycle (breathing difference within once cycle) variation affected by the subject's pose (De Troyer & Estenne 1984) and the breathing pattern (Sharp et al. 1975). Knowing that organ motion due to respiration is not repeatable (Benchetrit 2000), such modeling could replace gated NAC-PET, MRI or CT motion estimation. Note however that there is a close relation between using a motion model based on a surrogate and gating based on the same surrogate, see also below. The obtained models can be used for motion compensation in PET (PET/CT or PET/MRI), see Section 5.3. This has been done by either evaluating the motion model at the time of every event in the LM data (Livieratos et al. 2005b, Liu et al. 2011, Chan et al. 2013, Chan et al. 2018), or by gating the PET data according to the surrogate and using the motion model to compute an approximate motion field for each gate based on the average surrogate value for that gate (Manber et al. 2016).

Respiratory motion models can be divided in two categories: patient specific and population models.

4.2.1. Patient Specific When no a-priori respiratory motion information can be found and/or when no respiratory-based mathematical models are already built from an existing population, a patient specific motion model can be built. Such model will relates a surrogate (internal, external, data driven) to and internal motion extracted from images and will be based on a correlation between internal and external structures respiratory motion (Fayad et al. 2011).

In CT, 4-D volumes often contain artifacts due to inter-cycle variation and the need to bin the data in a predefined number of gates. Many patient specific motion models have been proposed in order to resolve these issues (McClelland et al. 2006, Ehrhardt et al. 2007, McClelland et al. 2010, Fayad, Pan, Pradier & Visvikis 2012, Sun &

Mok 2012, Zhang et al. 2013). These models relate the acquired external surrogate motion (pressure belt, real-time position management (RPM), surface information, or some markerless methods (Rostampour et al. 2018) to the internal structure motion (registration of 4-D CT images as shown in the previous section) and include therefore the possibility to model inter- and intra-cycle variations.

In MRI, motion can lead to blurring and respiratory motion compensation is necessary especially for thoracic and abdominal regions. An accurate motion modeling is required to make the necessary corrections (Gillman et al. 2017, Munoz et al. 2016). These models are divided into two categories; based on a motion correction implemented in a prospective way by scaling the magnetic field gradients during image acquisition in order to compensate for the effects of the motion on the acquired k-space data (Manke et al. 2003, Fischer et al. 2006, Baumgartner et al. 2017, Baumgartner et al. 2014, Celicanin et al. 2014, Ginn et al. 2019, Stemkens et al. 2016) or alternatively in a retrospective fashion from reconstructed dynamic MR or in combination with image reconstruction (Odille et al. 2008, Odille et al. 2010). These models can be used PET motion correction (Fayad, Schmidt, Würslin & Visvikis 2015, Manber et al. 2016, Küstner et al. 2017).

Motion models can also be estimated from the PET data. However, it is virtually impossible to reconstruct dynamic PET images at the required temporal resolution while still obtaining sufficient image quality for respiratory motion estimation. Moreover, the associated computational cost would also be very high. An alternative approach is to estimated the model parameters from gated NAC PET images. Such methods were first developed to relate organ-specific rigid motion to a (1-D) surrogate (Livieratos et al. 2005b, Liu et al. 2011, Chan et al. 2013) and later extended by fitting a voxel-specific linear model to the motion fields of each voxel obtained from registering phase-gated PET images (Chan et al. 2018). This approach was extended towards a 2D surrogate (displacement and velocity) where the PET data was histogrammed based on a 2D matrix, similar to dual-gating (Whitehead et al. 2020). As an alternative to using NAC PET images, Lu et al. (2018) used maximum-likelihood activity and attenuation correction factors estimation (MLACF) (Rezaei et al. 2014) to reconstructed gated AC PET images for the motion model estimation, as well as reference phase that best matches the CT image.

4.2.2. Population (Atlas-Based) In order to create patient specific models for diagnostic applications, there is an issue related to the increased dose associated with 4-D CT, which cannot be easily justified in all clinical scenarios. In 4-D MRI, the issue associated with the use of 4-D CT is irrelevant, given the non-ionising nature of MRI acquisitions. However, in MRI, the main concerns for motion modeling are the relatively long acquisition times associated with 4-D MRI which is often incompatible with clinical protocols and/or the MRI data collected with many of the advanced MRI techniques, such as tagged magnetic resonance imaging (TMRI) (Moore et al. 2000), cannot be used for clinical diagnosis. One of the possible solution to handle these issues is the creation

of population based respiratory motion model. Until now, this category is still under investigation and therefore is an active research area that have his direct Impact on imaging (PET/CT and PET/MR) but on therapy too (radiotherapy).

In CT, many population models have been previously developed (McQuaid et al. 2009, McClelland et al. 2017, Geimer et al. 2017, Fayad et al. 2018, Fayad, Buerger, Tsoumpas, Cheze-Le-Rest & Visvikis 2012, Wilms et al. 2017). These models have shown that motion estimation accuracy in the presence of inter-fraction motion variations can be improved using correspondence models that incorporate motion information from different patients. Surrogate information are either based on 1-D respiratory signal acquisition (McClelland et al. 2017) or on external surfaces acquired using time of flight based cameras (Fayad et al. 2018, Wentz et al. 2012) or internal features such as the diaphragm (McQuaid et al. 2009). In the latter case, the motion model was then fit to the PET data based on points in the diaphragm determined from NAC-PET images (McQuaid et al. 2011).

In MRI, some of the models were recently developed (Peressutti et al. 2013, Fayad, Buerger, Tsoumpas, Cheze-Le-Rest & Visvikis 2012). However, they still need further development and validation in order to be accepted as potential solution.

5. Motion Correction Techniques

This section introduces the basics of motion correction in PET image reconstruction. Motion correction techniques aim at using an estimation of the motion in order to produce motion artifact-free images.

Section 5.1 describes the statistical model and derives the log-likelihood function. Section 5.2 describes post-reconstruction registration (PRR) approaches, which consists of correcting for the motion by registering a sequence of images reconstructed at each time gate. Sections 5.3 and 5.4 respectfully describe MCIR approaches with pre-estimated motion and with motion estimated during the reconstruction.

5.1. Statistical Model

The 3-D activity and attenuation images are represented by column vectors $\boldsymbol{\lambda} \in \mathbb{R}_+^{n_\mathrm{v}}$ and $\boldsymbol{\mu} \in \mathbb{R}_+^{n_\mathrm{v}}$, n_v being the number of voxels in the image. The activity image $\boldsymbol{\lambda}$ is the parameter to be reconstructed while the attenuation image $\boldsymbol{\mu}$ is assumed to be already reconstructed, for example from CT or MRI.

We will use the following notations: $[\cdot]_i$ denote the i-th entry of a vector and $[\cdot]_{i,j}$ denotes the entry at the i-th row and at the j-th column of a matrix; '$^\top$' is the matrix transpose symbol; $\mathcal{L}(\boldsymbol{\vartheta} \mid \boldsymbol{x})$ denotes the log-likelihood of some parameter $\boldsymbol{\vartheta}$ given a random vector whose distribution is parametrized by $\boldsymbol{\vartheta}$; Id is the identity map.

5.1.1. Static Model The PET system is modeled with a $n_\mathrm{d} \times n_\mathrm{v}$ matrix $\boldsymbol{P}$, n_d being the number of detector bins (which may include TOF information), which includes the

geometry of the system and normalization factors; each entry $\boldsymbol{P}_{i,j}$ is the probability that an annihilation that occurred at voxel j is detected in detector bin i in absence of attenuation. At each detector $i = 1, \ldots, n_{\mathrm{d}}$, the detected events (counts) resulting from radioactive decay are usually modeled as independent homogeneous Poisson processes (i.e., time-independent) with rate Λ_i (in (decay-corrected) number of events per unit of time) defined by the activity and the attenuation as

$$\Lambda_i = a_i(\boldsymbol{\mu})[\boldsymbol{P}\boldsymbol{\lambda}]_i + r_i \tag{1}$$

where $a_i(\boldsymbol{\mu})$ is the attenuation factor of the i-th line of response (LOR), i.e.,

$$a_i(\boldsymbol{\mu}) = \exp\left(-[\boldsymbol{L}\boldsymbol{\mu}]_i\right) , \tag{2}$$

$\boldsymbol{L}$ being a $n_{\mathrm{d}} \times n_{\mathrm{v}}$ matrix that evaluates the line integrals of $\boldsymbol{\mu}$ along the LORs defined by each detector bin i (with incorporation of efficiency effects), and r_i is the background event (scatter and randoms) rate at bin i. The detections occurring during the time interval $[0, \tau]$ are modeled by a collection of independent random variables y_i, each of which following a Poisson distribution of parameter $\tau\Lambda_i$. For each bin i we have

$$y_i \sim \mathrm{Poisson}\left(\bar{y}_i(\boldsymbol{\lambda}, \boldsymbol{\mu})\right) \tag{3}$$

where $\bar{y}_i(\boldsymbol{\lambda}, \boldsymbol{\mu})$ is the expected number of detections at bin i, i.e.,

$$\bar{y}_i(\boldsymbol{\lambda}, \boldsymbol{\mu}) = \tau\left(a_i(\boldsymbol{\mu})[\boldsymbol{P}\boldsymbol{\lambda}]_i + r_i\right) . \tag{4}$$

Given the observed events $\boldsymbol{y} = [y_1, \ldots, y_{n_{\mathrm{d}}}]^\top$ and omitting terms independent of $\boldsymbol{\lambda}$, the HM log-likelihood of the activity image $\boldsymbol{\lambda}$ is

$$\mathcal{L}(\boldsymbol{\lambda} \mid \boldsymbol{y}) = \sum_{i=1}^{n_{\mathrm{d}}} L(y_i, \bar{y}_i(\boldsymbol{\lambda}, \boldsymbol{\mu})) \tag{5}$$

with $L(x, z) = x \log z - z$ and with convention $0 \cdot \log 0 = 0$.

The reconstructed AC activity image $\hat{\boldsymbol{\lambda}}$ is obtained from the observed data by maximization of the penalized log-likelihood, i.e.,

$$\hat{\boldsymbol{\lambda}} = \underset{\boldsymbol{\lambda} \geq \boldsymbol{0}}{\operatorname{argmax}}\, \mathcal{L}(\boldsymbol{\lambda} \mid \boldsymbol{y}) - U(\boldsymbol{\lambda}) \tag{6}$$

where U is an image regularization term. Optimization problem (6) can be solved with standard model-based image reconstruction (MBIR) iterative techniques such as the expectation-maximization (EM) algorithm (Shepp & Vardi 1982, Lange & Carson 1984) (without regularization) or its modified version (De Pierro 1995, Qi & Huesman 2006) (with regularization).

5.1.2. Model with Motion In this section we only consider HM-based motion-corrected PET. We assume that the PET raw data have been regrouped into n_{g} respiratory gates $\boldsymbol{y}_1, \ldots, \boldsymbol{y}_{n_{\mathrm{g}}}$ with no intra-gate respiratory motion. At each gate m, the respiratory motion from a reference state to the state at gate m is modeled by a 3-D spatial transformation $\boldsymbol{\varphi}_m$: $\mathbb{R}^3 \rightarrow \mathbb{R}^3$, to which we associate an image-to-image *warping operator* $\boldsymbol{\mathcal{W}}_{\boldsymbol{\varphi}_m}$ that maps the activity image $\boldsymbol{\lambda}$ and the attenuation image $\boldsymbol{\mu}$ to their

deformed versions $\boldsymbol{\mathcal{W}}_{\boldsymbol{\varphi}_m}\boldsymbol{\lambda}$ and $\boldsymbol{\mathcal{W}}_{\boldsymbol{\varphi}_m}\boldsymbol{\mu}$. This model assumes that there is no intra-gate motion. The warping operator can be implemented by modeling the image as a continuous object by interpolation (Blume et al. 2010) or using basis functions (Jacobson & Fessler 2003a, Jacobson & Fessler 2006, Bousse et al. 2016b).

Given the binned data $\{\boldsymbol{y}_m\}$ at each gate m, the new HM log-likelihood of $\boldsymbol{\lambda}$ and $\{\boldsymbol{\varphi}_m\}$ is (Bousse et al. 2016b)

$$\mathcal{L}(\boldsymbol{\lambda}, \{\boldsymbol{\varphi}_m\} \mid \{\boldsymbol{y}_m\}) = \sum_{m=1}^{n_\mathrm{g}} \sum_{i=1}^{n_\mathrm{d}} L(y_{i,m}, \bar{y}_{i,m}(\boldsymbol{\lambda}, \boldsymbol{\mu}, \boldsymbol{\varphi}_m)) \tag{7}$$

where

$$\bar{y}_{i,m}(\boldsymbol{\lambda}, \boldsymbol{\mu}, \boldsymbol{\varphi}_m) = \tau_m \left(a_i(\boldsymbol{\mathcal{W}}_{\boldsymbol{\varphi}_m}\boldsymbol{\mu})[\boldsymbol{P}\boldsymbol{\mathcal{W}}_{\boldsymbol{\varphi}_m}\boldsymbol{\lambda}]_i + r_{i,m} \right) , \tag{8}$$

$y_{i,m} = [\boldsymbol{y}_m]_i$ is the number of detections at bin i and gate m, τ_m is the total duration of the m-th gate, $r_{i,m}$ is the background event (scatter and randoms) rate at bin i and gate m and a_i was defined in Equation (2). The forward model (8) that accounts for the deformation of the LORs and attenuation correction factors (ACFs) can be computed through a "warp-and-project" approach, i.e., by first applying the motion to the activity image $\boldsymbol{\lambda}$ then by projecting, which does not require to store the motion-corrected system matrix $\boldsymbol{P}\boldsymbol{\mathcal{W}}_{\boldsymbol{\varphi}_m}$ (Jacobson 2006). Similarly, the ACF $a_i(\boldsymbol{\mathcal{W}}_{\boldsymbol{\varphi}_m}\boldsymbol{\mu})$ accounts for the motion of the attenuation map $\boldsymbol{\mu}$. Alternatively, the motion can be directly incorporated in the system matrix (Lamare, Cresson, Savean, Cheze-Le Rest, Reader & Visvikis 2007, Lamare, Carbayo, Cresson, Kontaxakis, Santos, Cheze-Le Rest, Reader & Visvikis 2007).

The HM log-likelihood $\mathcal{L}$ is a measure of goodness of the fit between the observed data $y_{i,m}$ and the expected data with motion $\bar{y}_{i,m}(\boldsymbol{\lambda}, \boldsymbol{\mu}, \boldsymbol{\varphi}_m)$ at each bin i and each gate m, that is to say $\mathcal{L}$ is maximized if at each gate m the deformed images $\boldsymbol{\mathcal{W}}_{\boldsymbol{\varphi}_m}\boldsymbol{\lambda}$ and $\boldsymbol{\mathcal{W}}_{\boldsymbol{\varphi}_m}\boldsymbol{\mu}$ the expected number of detections match with the projection data $\boldsymbol{y}_m$.

5.2. Post-Reconstruction Registration

PRR is achieved in a three-step process. Firstly, the reconstructed 3-D PET image $\hat{\boldsymbol{\lambda}}_m$ for each gate m is reconstructed from the gated data $\boldsymbol{y}_m$ using a static model (Section 5.1.1).

Secondly the reconstructed images $\hat{\boldsymbol{\lambda}}_m$ are either registered to a reference image $\hat{\boldsymbol{\lambda}}_{m_0}$ or resampled using a predetermined motion estimate (see Section 4). The registered/resampled image from gate m to gate m_0 is denoted $\hat{\boldsymbol{\lambda}}_{m,m_0}$.

Finally, the motion-corrected image $\hat{\boldsymbol{\lambda}}_\mathrm{prr}$ (at gate m_0) is defined as the weighted sum or similar of the motion corrected images:

$$\hat{\boldsymbol{\lambda}}_\mathrm{prr} = \sum_{m=1}^{n_\mathrm{g}} \alpha_m \hat{\boldsymbol{\lambda}}_{m,m_0} . \tag{9}$$

For optimal noise properties, the weights α_m should be proportional to the gate durations τ_m (Chun & Fessler 2013).

Possibly the first paper using PRR was by Klein et al. (1996) which used optical flow registration on cardiac-gated PET. Dawood et al. (2006) used optical flow on respiratory gated NAC images, but did not seem to specify how to handle attenuation. Kinahan et al. (2006) proposed to use demons registration on gated CT. Thorndyke et al. (2006) used B-spline registration on the reconstructed PET images. Since then, PRR has been applied in many different contexts, with more recently using registration from MR images (King et al. 2011, Dikaios et al. 2012, Würslin et al. 2013).

Various authors have suggested ways to cope with registration failures. Dikaios & Fryer (2012) used a global factor per gate based on mutual-information metrics. Thielemans, Gopalakrishnan, Roy, Srikrishnan, Thiruvenkadam, Wollenweber & Manjeshwar (2011) used local weights based on the deformation fields. The first version of Q.Freeze, the commercial product of GE Healthcare, used a median of the registered images as opposed to a sum.

PRR approaches are relatively simple to implement. However, they have several potential drawbacks. The single-gate reconstructed images suffer from attenuation correction artifacts as the attenuation map is not aligned with all the PET gates, unless matched attenuation (e.g., from cine CT, gated MR or warping via the determined motion) are available, see Section 5.7. In addition, the post-registration interpolation induces smoothing. On the other hand, the smoothing acts as (possibly unexpected) noise reduction (Polycarpou et al. 2012, Tsoumpas et al. 2013). The smoothing can be resolved by using super-resolution techniques (Wallach et al. 2012). Another drawback of PRR is that the gated images can suffer from bias due to the low-count data (Polycarpou et al. 2012, Tsoumpas et al. 2013).

5.3. Motion Correction Incorporated Reconstruction: Pre-estimated Motion

MCIR consists in reconstructing the activity image by maximization of the (penalized) log-likelihood (Equation (7)) with respect to $\boldsymbol{\lambda}$ using an estimate of the motion $\{\hat{\boldsymbol{\varphi}}_m\}$. This section describes MCIR techniques in which motion estimation and motion-corrected reconstruction are performed in two different steps.

In a first step, an estimate $\hat{\boldsymbol{\varphi}}_m$ of the true respiratory motion $\boldsymbol{\varphi}_m$ at each gate m is obtained, either by registering the gated reconstructed PET images in the same way as for PRR techniques, or with a motion model obtained from separate measurement (cf. Section 4).

In a second step, the image is reconstructed from the gated data $\{\boldsymbol{y}_m\}$ with incorporation of the estimated motion $\{\hat{\boldsymbol{\varphi}}_m\}$. This is generally achieved by maximization of the maximized log-likelihood with respect to $\boldsymbol{\lambda}$ and using the estimated motion $\hat{\boldsymbol{\varphi}}_m$, i.e.,

$$\hat{\boldsymbol{\lambda}}_{\text{mcir}} = \arg\max_{\boldsymbol{\lambda}} \mathcal{L}(\boldsymbol{\lambda}, \{\hat{\boldsymbol{\varphi}}_m\} \mid \{\boldsymbol{y}_m\}) - U(\boldsymbol{\lambda})\,. \tag{10}$$

When a reference gate m_0 is chosen for reconstruction then $\boldsymbol{\varphi}_{m_0} = \text{Id}$. Solving (10) can be achieved with the same iterative algorithms as for the static case (6) with the motion-corrected system matrices $\boldsymbol{P}\boldsymbol{\mathcal{W}}_{\boldsymbol{\varphi}_m}$ and ACFs $a_i(\boldsymbol{\mathcal{W}}_{\boldsymbol{\varphi}_m}\boldsymbol{\mu})$.

Early research on MCIR did not address the estimation of the motion but rather investigate the possibility of correcting for motion within an EM-like algorithm from HM or LM data (Qi & Huesman 2002, Rahmim et al. 2004, Livieratos et al. 2005a, Lamare, Cresson, Savean, Cheze-Le Rest, Reader & Visvikis 2007).

MCIR methods are in principle straightforward to implement, provided that the motion warps $\boldsymbol{\mathcal{W}}_{\boldsymbol{\varphi}_m}$ and $\boldsymbol{\mathcal{W}}_{\boldsymbol{\varphi}_m}^{\top}$ can be computed. Chun & Fessler (2013) have demonstrated when using *exact* motion $\{\boldsymbol{\varphi}_m\}$ MCIR always outperforms PRR in terms of variance, and the gap between the two approaches increases when the gates have significantly different duration. This suggest that MCIR is preferable to PRR. However, motion estimation errors may introduce further bias and/or variance into MCIR images and would reduce the gap between MCIR and PRR. To the best of our knowledge, the United Imaging Healthcare (UIH) HYPER FOCUS™ product is the only commercial implementation of an MCIR algorithm in PET. It uses motion estimates obtained by registering gated PET images to the single CT.

While MCIR is typically implemented in a HM-based reconstruction framework, it can also be implemented in LM-based reconstruction framework (Lamare, Cresson, Savean, Cheze-Le Rest, Reader & Visvikis 2007) using the same motion estimation. One advantage of LM-based correction is the potential of correcting intra-gate motion. Using the correlation between external motion signal acquired with high temporal resolution and internal organ movements, continuous motion information also with high temporal resolution can be derived in both rigid and non-rigid fashion. Subsequently, LM-based correction can be applied for event-by-event correction to eliminate intra-gate motion (Carson et al. 2003, Lamare, Cresson, Savean, Cheze-Le Rest, Reader & Visvikis 2007, Chan et al. 2013, Chan et al. 2018). Another advantage is that event-by-event correction provides unique opportunities for motion correction in dynamic PET (parametric imaging), while HM-based MCIR is more suitable for static PET (Yu et al. 2016). Note that for LM-based MCIR the warp-and-project approach does not suffice as the entries of the motion-compensated system matrix need to be computed individually for each event.

For rigid or affine motion, an alternative to the approach described above, *i.e.*, adapting the system matrix for the motion, is to precorrect the LM or HM data usually after normalising for detection efficiencies (Fulton 2001, Bloomfield et al. 2003). This approach, sometimes called "LOR-repositioning", has been used to correct for respiratory motion of (almost) rigid organs such as the myocardium (Livieratos et al. 2005c) and kidney (Chan et al. 2013), but is not further described here as it cannot handle the complex internal deformations due to respiration. See (Rahmim 2005) for a review of such methods related to brain imaging. For non-rigid respiratory motion , "curve-of-response" instead of "line-of-response" can be implemented in LM-based reconstruction for correction (Chan et al. 2018).

5.4. Motion Correction Incorporated Reconstruction: Joint Reconstruction and Motion Estimation

Instead of using a pre-estimated motion from a separate measurement, MCIR can estimate the motion from the gated PET projection data $\{\boldsymbol{y}_m\}$ within a joint estimation of $\boldsymbol{\lambda}$ and $\{\boldsymbol{\varphi}_m\}$ by maximization of the penalized log-likelihood:

$$(\hat{\boldsymbol{\lambda}}_{\text{mcir}}, \{\hat{\boldsymbol{\varphi}}_m\}) = \underset{\boldsymbol{\lambda}\geq\boldsymbol{0},\, \{\boldsymbol{\varphi}_m\}}{\arg\max}\, \mathcal{L}(\boldsymbol{\lambda}, \{\boldsymbol{\varphi}_m\} \mid \{\boldsymbol{y}_m\}) - V(\{\boldsymbol{\varphi}_m\}) - U(\boldsymbol{\lambda}) \tag{11}$$

where we assumed a parametric model for $\boldsymbol{\varphi}_m$ and V is a regularization term for $\{\boldsymbol{\varphi}_m\}$—which can incorporate temporal regularization. In other words, this approach estimates a deformation field such that the activity and attenuation images match the PET projection data. We refer to this approach as joint reconstruction and motion estimation (JRM). The main advantage of JRM compared to other MCIR is that it does not require additional hardware to measure the motion.

A reference gate m_0 can be chosen for the reconstruction, in which case $\boldsymbol{\varphi}_{m_0} = \text{Id}$; this assumes that the attenuation map $\boldsymbol{\mu}$ is aligned with the PET data at gate m_0. Contrary to the previous methods where the motion is estimated separately, imposing a reference gate is not a requirement as reconstructed activity $\hat{\boldsymbol{\lambda}}_{\text{mcir}}$ is warped alongside $\boldsymbol{\mu}$ with the estimated motion $\{\hat{\boldsymbol{\varphi}}_m\}$.

Solving (11) can be achieved by iteratively alternating between maximization in $\hat{\boldsymbol{\lambda}}$ and $\{\boldsymbol{\varphi}_m\}$ until convergence. More precisely, given the current estimate of the activity $\boldsymbol{\lambda}^{(q)}$ and of the motion $\{\boldsymbol{\varphi}_m^{(q)}\}$ at iteration q, the new estimates at iteration $q+1$ are

$$\{\boldsymbol{\varphi}_m^{(q+1)}\} = \underset{\{\boldsymbol{\varphi}_m\}}{\arg\max}\, \mathcal{L}(\boldsymbol{\lambda}^{(q)}, \{\boldsymbol{\varphi}_m\} \mid \{\boldsymbol{y}_m\}) - V(\{\boldsymbol{\varphi}_m\})\,, \tag{12}$$

$$\boldsymbol{\lambda}^{(q+1)} = \underset{\boldsymbol{\lambda}\geq\boldsymbol{0}}{\arg\max}\, \mathcal{L}(\boldsymbol{\lambda}, \{\boldsymbol{\varphi}_m^{(q+1)}\} \mid \{\boldsymbol{y}_m\}) - U(\boldsymbol{\lambda})\,. \tag{13}$$

While the maximization in $\boldsymbol{\lambda}$ (Equation (13)) was addressed in Section 5.3, solving Equation (12) is more challenging as it corresponds to a registration task in the PET projection space.

In a simple 2-D setting without attenuation correction, Jacobson & Fessler proposed a joint estimation approach where Equation (12) is solved by optimization transfer techniques (Jacobson & Fessler 2003b, Jacobson 2006). These techniques are designed such that motion estimation is carried out in the image space with "temporary" images, similarly to an image registration task at each gate, thus avoiding successive projections with the system matrix $\boldsymbol{P}$. In a similar setting but with 3-D images, Blume et al. (2010) then Blume et al. (2012) utilized a gradient ascent technique to directly solve (12).

Accounting for the simultaneous deformation of the activity and the attenuation is more challenging. Bousse et al. proposed a joint estimation framework for PET/CT that accounts both deformed images using a quasi-Newton algorithm to solve (12), where the estimated motion jointly warps the activity $\boldsymbol{\lambda}$ and the attenuation $\boldsymbol{\mu}$ such that they both match to the data $\{\boldsymbol{y}_m\}$ (Bousse et al. 2016b, Bousse et al. 2016a). This framework does not require a reference gate m_0 as the reconstructed activity and the attenuation are automatically aligned and deformed simultaneously—the attenuation is not required

to be aligned with any of the PET gates. In principle, this framework requires an attenuation map with accurate attenuation values. However, they observed in a more recent paper that motion estimation is robust to localized errors in the attenuation image and that it could be applied to PET/MRI using an MRI-derived attenuation map (Bousse et al. 2017).

The motion model can also include the Jacobian of the motion for mass preservation for the activity and the attenuation. It was reported in Émond et al. (2020) the quantification in compressible areas such as the lungs can be improved with a mass-preserving motion model.

5.5. Motion Correction via (De)convolution

The above approaches use transformations between several gates to either motion correct (Section 5.2) or model the motion (Section 5.3). A less common approach is to model the blurring caused by the motion via convolution. This was first proposed by Menke et al. (1996) in the context of rigid head motion. Local blurring kernel were derived from a motion tracker and then used to (locally) deconvolve the motion-corrupted image. However, this can increase noise. Siemens's OncoFreeze™ chooses a reference gate, typically the HD-Chest™ gate (see Section 3.3), and estimates motion blurring between the reference gate and the ungated (and hence blurred) reconstruction using optical flow. This motion blurring is then used in reconstruction similar to a point spread function (PSF) implementation (Hong et al. 2014). Karakatsanis et al. (2017) developed a similar method but accelerated convergence by using a nested EM Lucy-Richardson deconvolution algorithm for motion compensation. The PSF approach is less sensitive to noise amplification than deconvolution, and allows using all detected events. However, the effect of attenuation mismatch (see Section 5.7) is currently less understood.

5.6. Examples of Motion-Corrected PET Images Obtained using MCIR Techniques

Figure 5 and Figure 6 show examples on motion-corrected reconstructed PET images from Bousse et al. (2017). These images show that MCIR can significantly reduce the motion blur as well as revealing a lesion that was invisible in the uncorrected image.

Figure 7 shows another example of the effect of motion correction, this time from Manber et al. (2015). Uncorrected PET images suffers from attenuation correction artifacts due to the misalignment of the attenuation map with the respiratory-gated PET data, while the motion correction realigns the attenuation map to each of the respiratory gates, resulting in artifact-free images.

JRM techniques have the advantage of operating on raw gated PET only, thus removing the need of additional measurements. Blume et al. (2010) and Bousse et al. reported that JRM delivers images with a better bias/variance than with PRR. This is due to the fact that PRR performs registration on individually reconstructed images

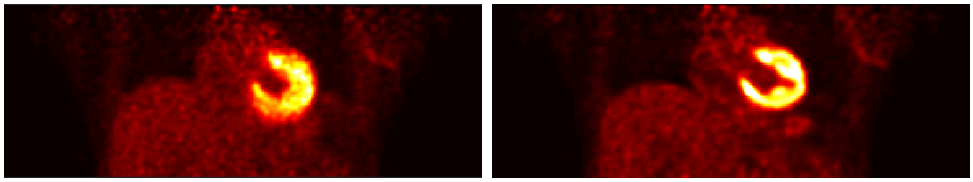

(a) (b)

Figure 5: PET coronal slice images reconstructed from Siemens Biograph mMR PET/MRI data: (a) without motion correction and (b) with motion correction. In absence of motion correction, the reconstructed image suffers from motion blur, while the motion blur is significantly reduced in the motion-corrected image. Reprint from Bousse et al. (2017).

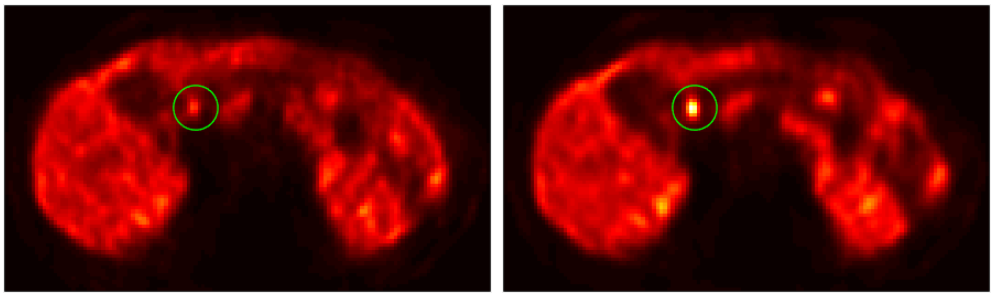

(a) (b)

Figure 6: PET trans-axial slice images reconstructed from Siemens Biograph mMR PET/MRI data: (a) without motion correction and (b) with motion correction. The green circle indicates the location of a hot lesion. Reprint from Bousse et al. (2017).

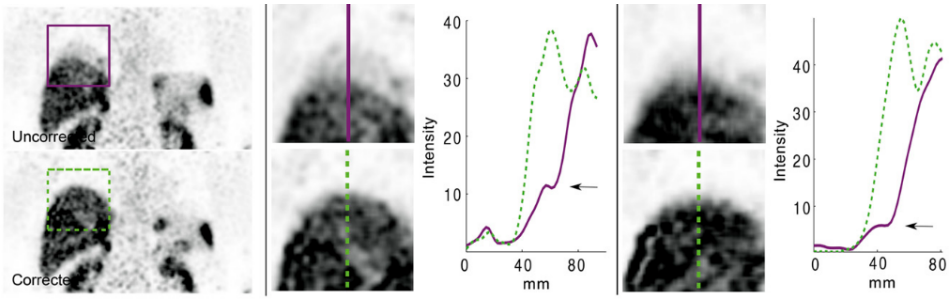

Figure 7: Comparison between uncorrected (top row with purple line profile) and motion-corrected (bottom raw with dotted green line profile) reconstructed PET images. Reprint from Manber et al. (2015).

where the noise is amplified by the reconstruction, while JRM operates in the projection space.

Despite these advantages, JRM techniques are computationally expensive as the motion update step (12) require to compute $\boldsymbol{H}$ and $\boldsymbol{H}^\top$ at each gate, while other methods estimate the motion in the image space.

5.7. Attenuation correction issues

PET data are typically acquired over a few minutes, while state-of-the-art CT scan takes only a few seconds, usually with patients holding breath. Even if CT data are acquired during free-breathing, the mismatch between time-averaged PET and snapshot CT data could still be significant. Not only affecting ungated static PET, such CT-PET mismatch also affects respiratory motion correction techniques described above as the reconstruction of gated PET images also suffers from mismatched attenuation correction, depending upon respiratory location where CT data are acquired (cf. Figure 7). Lu et al. (2018) showed that mismatched attenuation correction for each gated image results in errors in motion vector estimations among gates, subsequently degrading the final LM-based motion compensated image reconstruction results as the motion vectors are incorporated into motion correction. While gated images without attenuation correction could be used for motion estimation without the impact of mismatched attenuation correction (see Section 4.1), Lu et al. showed that motion vectors in region in the center of the human body, such as the spine, are not accurate for some tracers, due to the low apparent tracer concentration in those regions without attenuation correction. Therefore, ideally, matched attenuation correction should be performed for each gated image to ensure accurate motion vectors for motion compensation in the subsequent steps.

Facilitated by TOF information, it is now feasible to reconstruct both PET activity images and attenuation maps or ACFs directly from PET raw data without CT (Defrise et al. 2012, Panin et al. 2013, Rezaei et al. 2012), leading to perfectly matched attenuation correction. Though the quantitative accuracy of such approaches still requires further improvement, maximum-likelihood attenuation and activity estimation (MLAA) or MLACF could be used to generate gated images without mismatch artifacts to estimate accurate motion vectors. In Lu et al. (2018), the gated PET emission images generated by MLACF provided the most accurate motion vectors and subsequently led to superior final motion correction as compared to using motion vectors derived from NAC or CT-AC gated images. Although MLAA and MLACF framework theoretically do not require CT information, the majority of PET scanners nowadays are hybrid PET/CT with CT data readily available. To take advantage of the available CT information, Rezaei et al. (2016) developed an approach to simultaneously reconstruct the activity image and the transformation that warps the acquired CT attenuation map to match the activity image for matched attenuation correction. Such process can be applied to each gated image to achieve phase-matched attenuation correction for each gate. This approach is similar to that of Bousse et al. (2016b) and Bousse et al. (2016a), although it does not apply the deformation field to the activity image.

MLAA approaches are capable of generating attenuation maps. However such attenuation maps are noisy as they are derived from emission data. The noise in attenuation maps could be propagated into attenuation correction, in particular if MLAA is performed for each gate with only a fraction of detected events. Hwang et al.

(2018) recently developed a deep learning based approach. The inputs of convolutional neural network (CNN) are both activity and attenuation images from MLAA, while the label is CT-based attenuation map. Such a deep learning network is shown to be successful in generating low-noise attenuation maps that is consistent with CT-based attenuation map. Following these developments, Shi et al. (2019) further incorporated the line-integral of attenuation coefficients as additional loss function terms. Such implementation with PET physics information provided synthetic attenuation maps that is more consistent with CT-based attenuation maps. These deep learning based approaches can be directly applied to MLAA outputs of each individual gate to generate phase-matched attenuation maps, leading to phase-matched attenuation correction and subsequently more accurate motion vector estimations for motion compensation.

Although PET and CT have intrinsic respiratory mismatch due to different scan durations, there are efforts to make them match. Pan et al. (2006) proposed an approach to acquire time-averaged CT through cine CT acquisition. The resulting CT data are a motion blurred CT that matches with the respiratory blurriness of PET. Although this approach can not be used for diagnostic purposes, such CT is able to provide phase-matched attenuation correction for the gated PET.

Several authors have suggested methods to select part of the PET data where the patient is in the same respiratory state as during the CT (Chang et al. 2010, Meier et al. 2019, Hamill et al. 2020). However, in the context of motion correction, such an approach can not be used to generate phase-matched gated PET. Nevertheless, these methods could achieve a good reference image that can be used for other approaches, e.g., OncoFreeze (see Section 5.5) was used by Hamill et al. (2020).

5.8. Issues with Other Data Corrections

For accurate quantification in PET, accidental coincidences and scatter need to be taken into account, either via precorrection for analytic algorithms or by incorporating them into the acquisition model.

It is generally accepted in the literature that the distribution of the accidental coincidences does not depend on the motion state. This can be understood by the fact that it is determined by the underlying distribution of the singles, which will be very insensitive to motion as in present day PET septa are no longer used.

The effect of motion on the scatter distribution has not been well-studied in the literature to the best of our knowledge. As the scatter distribution in PET is very smooth, many authors assume that it is independent of motion (Manber et al. 2015, Chun, Reese, Ouyang, Guerin, Catana, Zhu, Alpert & Fakhri 2012). This was confirmed for head movement up to $\sim$2 cm for non-TOF PET (Thielemans 2005). Arm movement was studied in (Lodge et al. 2011).

If the scatter is independent of motion, it can be found from the ungated data and simply scaled for every gate. As an alternative, it is possible to find the scatter estimate for every gate independently. However, this makes the scatter estimate sensitive to noise.

In addition, model-based scatter estimation methods that scale the scatter estimate to "tails" without scatter can be sensitivity to motion, see e.g. (Anton-Rodriguez et al. 2010) for the head and (Callahan et al. 2012) for the arms. However, this is unlikely to be a problem for respiratory motion due to the small expansion of the chest. We are not aware of any studies investigating the impact of misaligned attenuation due to respiratory motion on model-based scatter.

In summary, respiratory motion is unlikely to affect scatter estimation in clinical practice. Nevertheless, further investigation is warranted, especially for systems with with increased TOF resolution.

6. Combining Respiratory Motion Correction with other Physiological Aspects

6.1. Dual Respiratory and Cardiac Gating and Motion Correction

In cardiac PET, the images are not only affected by respiratory motion, but also cardiac motion due to myocardium contraction. Therefore, simultaneously correcting both respiratory and cardiac motion is needed. Typical clinical cardiac SPECT and PET studies routinely use electrocardiogram (ECG) signals to bin data into 8 or 16 cardiac phase gates. Such cardiac gating trigger information can be directly combined with above-mentioned respiratory signals, either detected by external device or data-driven techniques, to facilitate corrections of both respiratory and cardiac motion.

With both a respiratory signal and cardiac triggers, PET LM data can be rebinned into "dual gates", each corresponding to a unique combination of respiratory phase and cardiac phase. Similar to motion estimation among respiratory gates, motion vectors mapping all dual respiratory-cardiac gates to a reference gate can be obtained using non-rigid image registration. Since cardiac contraction changes the myocardium thickness, the brightness of the images across cardiac gates are different, though the total tracer activity in the total myocardium stays the same. Therefore, registration methods based on the assumption of consistent brightness no longer apply to cardiac gated images. Gigengack et al. (2012) proposed an approach of image registration with mass-preserving to address this issue and applied to [^{18}F]fluorodeoxyglucose ([^{18}F]FDG) dual-gated images. All the dual-gated images registered to a reference gate were averaged to generate a motion correction cardiac PET image using all the data (PRR), thus the noise levels stay the same as the ungated motion blurred images. In addition to the PRR approach, Feng et al. (2016) compared three motion correction approaches for dual-gated PET, including motion corrections after reconstruction (i.e., PRR) similar to the implementation by Gigengack et al., by incorporating motion vectors in the system matrix (i.e., MCIR), and before (i.e., motion correction before reconstruction (MCBR)) image reconstructions using simulated [^{18}F]FDG PET data with phase-matched attenuation correction. The results showed that PRR and MCIR are both superior to MCBR, while MCIR is slightly better than PRR. Lamare et al.

(2014) reached the same conclusions with simulated dataset of the NCAT phantom and a clinical evaluation on 7 patients, by comparing four different schemes of combining dual-gated PET data, with additionally comparing an affine and a non-rigid elastic registration algorithm for the MCIR or PRR. The motion blurring between a reference gate, which could be one cardiac gate or dual gate, and the static motion blurred image can also be estimated to form motion blurring kernels. Similar to the OncoFreeze approach (Section 5.5), such motion kernels are incorporated into iterative reconstruction in the Siemens CardioFreeze™ package for motion deblurring of cardiac PET images using all detected events (Bendriem et al. 2018). In addition to [^{18}F]FDG studies, dual-gated PET methods were also applied to [^{18}F]Flurpiridaz, a promising perfusion tracer with high extraction fraction. Slomka et al. (2015) demonstrated that dual-gating provided the highest contrast and thinnest myocardium wall thickness as compared to either cardiac gating only or end-expiration gating only.

Each respiratory gate only includes a fraction of detected events, resulting in increased image noise. Each dual-gated image includes a further reduced fraction of counts. For example, a dual gating strategy with 5 respiratory gates and 5 cardiac gates would generate 25 dual gates, each with only 4% of counts. The high image noise could affect the accuracy of motion vector estimation, subsequently degrades motion correction. In the above mentioned paper by Gigengack et al., all patients underwent a hyperinsulinemic euglycemic clamp technique before and during the scan to enhance [^{18}F]FDG uptake in the heart, which is not a common practice. In certain patient populations, such as sarcoidosis, the myocardium [^{18}F]FDG update could be low thus making it hard to estimate motion vectors from PET data. If cardiac gated CT is available, cardiac motion can be derived from that, while respiratory motion can be found from respiratory gated PET data (Klén et al. 2016). Another way to address this challenge is to take advantage of MRI data in the simultaneously acquired PET/MRI cardiac PET studies. For example, Robson et al. (2018) described approaches to register respiratory and cardiac gated data to a reference gate and average them to achieve motion correction using the PRR approrach. The motion vector fields were derived from respiratory and cardiac gated MRI data, which were acquired during free breathing over several minutes and k-space lines were binned accordingly. The results showed robustly improved myocardium [^{18}F]FDG contrast for a cohort of patients with various [^{18}F]FDG patterns. In addition averaging transformed images, motion information derived from free-breathing MRI data can also be incorporated into the MCIR framework (Kolbitsch et al. 2017). While several studies used gradient-echo MRI sequences to generate gated MRI data, Munoz et al. (2019) presented an approach to use dual-phase coronary magnetic resonance angiography (CMRA) data to derived motion vectors to deform the attenuation maps for attenuation correction and estimate motion vectors to facilitate final motion correction, allowing visualization of the coronary arteries from CMRA data, which simultaneously provided motion correction information. While PET motion correction using motion information from MRI data has been investigated by many groups, Kolbitsch et al. (2018) presented an approach to take advantage of both

dual gated 4-D MRI and 4-D PET data through joint image registration. As shown in Figure 8, the joint PET-MRI motion estimation provided more accurate motion estimation than using either modality separately, which were incorporated into MCIR for final motion correction with phase-matched attenuation correction. In addition to applying MR-based dual motion correction to static PET, Petibon et al. (2019) also applied such approaches to dynamic [^{18}F]FDG PET and demonstrated 18% increase in K_i values in the septum as compared to without motion correction.

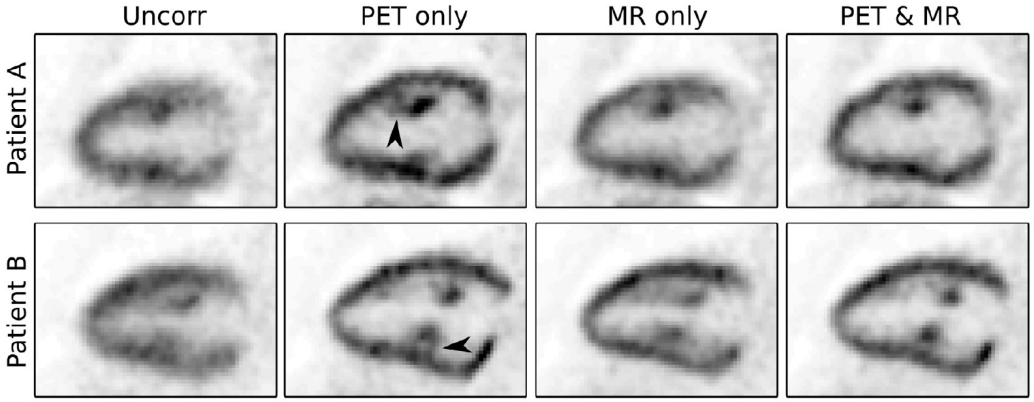

Figure 8: Long-axis slices of two patients comparing PET images without motion correction (Uncorr) and with cardiac and respiratory motion correction using motion fields obtained using only PET images (PET only), using only MR images (MRI only) and the proposed joint PET-MRI motion estimation (PET & MR). Artefacts (black arrows) and residual motion blurring is visible for motion correction based on PET only and MRI only images. (Phys. Med. Biol. 64 (2019) 015007)

Although much progress has been made in simultaneous respiratory-cardiac corrections for cardiac PET and PET/MR, most work has been done for ^{18}F labeled tracers, such as [^{18}F]FDG, Flurpiridaz, and NaF. One of the most widely used cardiac PET procedures is quantification of myocardial blood flow using flow tracers with high extraction fraction such as ^{82}Rb. Due to its short half life of 75 seconds, ^{82}Rb studies can only be performed with an on-site generator next to the scanner and images are typically noisy, posing unique challenges for motion correction. Because the ^{82}Rb generator can not be operated in a PET/MRI scanner room, the above mentioned MRI guided motion correction methods are not applicable as no ^{82}Rb PET studies can be performed using a PET/MRI scanner. In addition, due to the short half life and high image noise, motion vector estimation from dual-gated ^{82}Rb images could be very challenging. Therefore, further studies are urgently needed to develop dual motion correction methods for cardiac PET with short half-life perfusion tracers like ^{82}Rb.

6.2. Motion Correction and Kinetic Modeling

Kinetic modeling consists of applying a kinetic model to a dynamic sequence of PET images or time frames, either during the reconstruction of the dynamic data or on the reconstructed images as an image-based analysis. This process allows to extract kinetic parameters for specific regions, or parametric images, in order to derive more meaningful physiological information than with standard static imaging. Numerous linear or non-linear models exists for different radiotracers and have been discussed in multiple reviews (Rahmim et al. 2009, Reader & Verhaeghe 2014, Gallezot et al. 2018, Wang et al. 2020). As the calculations of kinetic parameters are based on the frame time-activity curves and respiratory motion quantitatively impacts the estimated activity in the images, the correction of respiratory motion can be crucial for various kinetic modeling applications.

The most immediate consequence of respiratory motion is that the activity under-estimation in the regions or voxel of interest due to the blurring effect of respiratory motion will result in the under-estimation or over-estimation of kinetic parameters. These effects can be important if the area of interest is located in the torso-abdominal region, which is the most affected by respiratory motion. For example in dynamic cardiac acquisitions, respiratory motion generally increases apparent wall thickness and decrease contrast to noise ratio and net influx rate estimation.

Another hindrance due to the long acquisitions usually required in dynamic studies, it is more likely to observe changes of patient breathing pattern and amplitude along the acquisition. This increases the probability of voxels misalignments outside/inside a specific region, resulting in a mismatch in the time-activity curve baseline. As example for the estimation of myocardium parametric images, motion can result in over-estimation of kinetic parameters in the regions of interest as voxels are relocated outside the myocardium region, leading to underestimation and overestimation of K_i and volume of distribution maps respectively (Gallezot et al. 2018). For the assessment of coronary flow reserve (CFR), when vasodilators are administered, the breathing pattern of the patients can change significantly, with higher amplitude during the stress scan. This can lead to errors in myocardial blood flow estimation and lead to a wrong assessment of CFR as observed in (Yu et al. 2016).

Additionally, most kinetic models require the knowledge of the input function, corresponding to the activity concentration in plasma, which is usually extracted from arterial or blood samples, estimated with a population-based approach, or estimated directly from the images following regions of interest such as the aorta, left ventricle or carotid artery. Through it is not available for all radiotracers dynamic studies, the last approach has the advantages of not being invasive and removing the need of pre-recorded data required for a population approach. However, respiratory motion will also affect the shape of image-derived input function the same way it affects time-activity curves. Irregular motion pattern could also cause mismatch between the input function ROIs in the early and late frames, requiring scaling or correction of the extracted image derived input function (IDIF) (Gallezot et al. 2018).

For direct parametric image reconstruction, several works explored the use of multiple kinetic/dynamic models order to avoid bias propagation from areas which doesn't fit the primary kinetic model (Kotasidis et al. 2011). These approaches aim to apply the kinetic model to a specific area or specific voxels through the use of adaptive (Kotasidis et al. 2014) or hybrid (Germino et al. 2014) strategies. The correction of respiratory motion can be crucial in this context as a voxel could overlap areas which fit or not the kinetic model depending on the motion.

Respiratory motion correction methods must address an additional challenge in the context of dynamic acquisition. As the available statistics for the reconstruction of each frame is often limited by the high temporal resolution restriction, in particular for early frames, the reconstructed frames often suffer from poor SNR. The use of pure gating methods which uses a fraction of the acquired data would further decrease it. It is therefore required to use methods which makes use of most of the statistics available in the acquisition, such as post-reconstruction registration or motion compensated image reconstruction techniques which make use of all events to reconstruct the data with gating approaches. Nevertheless, these methods do not deal with intra-gate motion, nor with the cases of irregular breathing patterns along the dynamic acquisition which can penalize any motion correction methods without proper handling of inter-cycle variations. This is however taken into account by event-driven gating methods which have been used for the reconstruction of dynamic acquisitions using the internal-external motion correlation method (INTEX) (Chan et al. 2013, Chan et al. 2018, Yu et al. 2016) (see Section 4.2). The correlation can be determined based on respiratory gated images of longer duration, starting after the initial bolus (Emond et al. 2019).

For the methods that use a data-driven method for extraction of the respiratory signal (Section 3.1), the quick tracer distribution in the early frames changes can significantly affect the respiratory traces. For PCA, the principal components of the tracer dynamics could dominate the respiratory motion in the beginning of the acquisition which makes the use of this technique unreliable for modeling studies which require early data (Ren et al. 2019). For COD, the mean tracer distribution change can be removed from the signal, however in the context of low activity and quick tracer kinetics, the respiratory information estimated with COD method can be unreliable as well (Ren et al. 2017). Therefore, while the data-driven approaches are promising as they prevent the requirement of an external surrogate device, further investigations are required to study methods to account for the high and low frequency changes (tracer arrival and washout) introduced by the tracer kinetics and affecting the event-driven signal.

For all those methods, it is also worthy to note that motion correction can also lead to erroneous kinetic parameters estimation due to local errors in the motion correction field (Petibon et al. 2019).

6.3. Gross body motion

Gross body motion, or bulk motion, is different in nature from respiratory motion as its timing is unpredictable. The movement can be an abrupt change of position, either due to a physiological cause such as coughing, or if the patient voluntary or involuntarily adjusts their position, or manifests as a gradual and progressive drift during the acquisition. Generally, longer acquisition increases the probability of higher amplitude of patient body motion. As for respiratory motion, body motion can be problematic for dynamic studies, causing under and over-estimation of kinetic parameters as a same voxel may represent different anatomical location of the patient along the scan, as shown for example for [^{18}F]FDG net influx rate (K_i) study (Gallezot et al. 2018, Lu et al. 2019) or myocardial blood flow (Hunter et al. 2016, Piccinelli et al. 2018).

Patient motion correction has been primarily investigated for SPECT studies, in particular for head and cardiac acquisitions. Lee & Barber (1999) initially proposed an iterative algorithm which estimates tangential/axial translations by registering forward projection of initial estimated images to the measured data. This approach was expanded in later studies (Kyme et al. 2003, Röhl et al. 2007, Schumacher et al. 2009, Bai et al. 2009). In order to detect rigid discrete motion, it has also been suggested to use cross-correlation or similar metrics between sinogram data acquired at different time points for SPECT (Pellot-Barakat et al. 2001) and CT (Ens et al. 2010). In brain PET, many groups proposed to apply rigid transformation with various techniques such as LOR rebinning (see for example (Menke et al. 1996, Bloomfield et al. 2003, Buhler et al. 2004)), Multi Acquisition Frame methods (e.g. (Picard & Thompson 1997, Fulton 2001, Mourik et al. 2009)) or joint-estimation approaches (e.g., (Jiao et al. 2017)).

Patient body motion correction has been less extensively studied than head motion, and differs from the latter as being mostly elastic. The correction methods generally used for head motion are therefore not applicable for an accurate correction of body motion, due to being restricted to rigid motion correction. As for respiratory motion correction, patient body motion can be detected using either external devices or high temporal resolution MR images for PET/MRI systems (Gillman et al. 2017), or data-driven approaches. For the latter, COD method has been used to correct for body motion in multiple human and monkey analysis in Lu et al. (2019). If for respiratory motion detection, the anterior-posterior (CODy) and superior-inferior (CODz) components of the COD signal were primary used, the lateral trace (CODx) proved to be more efficient for the detection of body motion. Additionally, lower frequency (1 s by frame) was used to compute the COD signal. PCA may also be able to detect body motion, although assessing the magnitude of body motion should be less straightforward than with COD (Ren et al. 2019). Data-driven approaches have the advantage of not requiring any devices to estimate the motion and can be used to detect both respiratory and body motion. Further work is required on the optimal parameters for the data-driven approaches, in particular in the early frames of dynamic acquisitions in which the quick

kinetic changes might disrupt the motion detection from the signal.

A first approach to correct for body motion is frame-based image registration, which consists in separating the acquired data into multiple temporal frames in which the data is assumed to be motionless. Each frame is registered to a reference position during reconstruction. A major issue of this approach is that it does not correct for motion occurring within the predefined frames which can be problematic, in particular in the presence of a progressive drift. Its combination with respiratory motion correction using gating techniques is also complicated as gating techniques require a rebinning of the data into respiratory gates. Unless the gating could be performed within each body motion frames, the association of these methods for dual body and respiratory motion correction is challenging.

Gross-body movement has also been corrected using the convolution approach (Section 5.5) handling both respiratory and body motion (Karakatsanis et al. 2017), which led to improvement in K_i estimation for whole-body dynamic acquisitions. Lucy-Richardson deconvolution algorithms are known to reduce the signal to noise ratio and generate ring artifacts with deconvolution iterations so this approach require fine tuning of the deconvolution parameters along with potential denoising techniques for a practical use.

As several works explored event by event motion correction for respiratory motion correction, the same approach was studied for body motion correction (Lu et al. 2019). This method uses a data-driven approach (COD) for the detection of body motion, estimate the motion parameters through elastic image registration to generate motion vector fields, which are then applied in a non-rigid motion compensation ordered-subsets EM LM algorithm. This approach has the advantage to correct for body inter-frame and intra-frame body motion in a non-rigid manner, and allows a straightforward combination with respiratory motion correction. However, as mentioned previously for dynamic acquisitions, if the data-driven approach is retained for motion estimation instead of external devices or internal-external motion correlation methods, further work is required to improve the estimation of motion in the early frames of the dynamic acquisition.

7. Perspectives

Respiratory motion compensation in multimodality imaging has seen numerous advances over the past couple of decades motivated by the advent of multimodality imaging with PET/CT to start with, followed by PET/MR imaging. A large majority of the developments around respiratory motion compensation realized during the PET/CT era were subsequently transposed in the PET/MR multimodality imaging field. More specifically the developments during the last few years have concentrated on rendering the implemented methodologies transparent and more user friendly within the clinical acquisition framework in order to enable their implementation and acceptance in routine clinical practice.

The development of increasing axial field of view PET devices has recently led to a renewed interest in dynamic whole body quantitative parametric imaging (Slart et al. 2021). Within this context the integration of multiple physiological motion sources (respiratory, cardiac, radiotracer) during the reconstruction process will be undoubtedly a field that will receive extra attention in the future. These devices are also associated with an improved sensitivity and therefore the potential to improve temporal sampling and image quality for short time frames. As a consequence, adapting the already available respiratory compensation approaches will be part of the future developments in the field. One could imagine that in the future we could perhaps also revisit the initial idea of breath-holding PET acquisitions (Nehmeh et al. 2007) if the imaging systems' performance continues their impressive improvements of the past few years.

The inconveniences, in terms of a smooth clinical workflow, associated with the use of direct measuring devices of respiratory motion in combination with the magnetic field incompatibility issues (of interest in combined PET/MR devices) has led to an increased interest in the generic patient model based approaches. In most of these, a surrogate measure of respiratory motion is used in combination with a 3-D acquisition in order to obtain a 4-D image series or directly the corresponding 4-D displacement matrices used in the implementation of motion compensation strategies (see Section 4.2). This is clearly a field where artificial intelligence can play a role in the future in order to allow an improvement in both the precision and computational efficiency of existing model based solutions (Li et al. 2020). Beyond this specific application, artificial intelligence may be also employed at different stages of the respiratory motion compensation strategies, including denoising (in image or raw data space) of low dose respiratory gated frames, cross-modality 4-D image generation, as well as in 4-D image reconstruction.

Finally, what is still greatly missing is a rigorous assessment of clinical impact for the use of respiratory compensation approaches in multimodality imaging. This has been hampered in the past by the complexity of the proposed solutions and the fact that the vast majority of clinical PET applications concern tumor detection where respiratory motion management may play a role but not significant enough to justify the additional effort. The combination of mainstream data driven motion compensation approaches and the increase of therapy assessment studies in PET imaging may provide in the future the necessary framework for demonstrating the clinical interest of respiratory motion management.

References

Abdelnour, A. F., Nehmeh, S. A., Pan, T., Humm, J. L., Vernon, P., Schöder, H., Rosenzweig, K. E., Mageras, G. S., Yorke, E., Larson, S. M. & Erdi, Y. E. (2007). Phase and amplitude binning for 4D-CT imaging, *Physics in Medicine and Biology* **52**(12): 3515–3529.

Alnowami, M., Alnwaimi, B., Tahavori, F., Copland, M. & Wells, K. (2012). A quantitative assessment of using the Kinect for Xbox 360 for respiratory surface motion tracking, *Medical Imaging 2012: Image-Guided Procedures, Robotic Interventions, and Modeling*, Vol. 8316, International Society for Optics and Photonics, p. 83161T.

URL: *https://www.spiedigitallibrary.org/conference-proceedings-of-spie/8316/83161T/A-quantitative-assessment-of-using-the-Kinect-for-Xbox-360/10.1117/12.911463.short*

Anton-Rodriguez, J. M., Sibomana, M., Walker, M. D., Huisman, M. C., Matthews, J. C., Feldmann, M., Keller, S. H. & Asselin, M. (2010). Investigation of motion induced errors in scatter correction for the HRRT brain scanner, *IEEE Nuclear Science Symposuim Medical Imaging Conference*, pp. 2935–2940. ISSN: 1082-3654.

Bai, C., Maddahi, J., Kindem, J., Conwell, R., Gurley, M. & Old, R. (2009). Development and evaluation of a new fully automatic motion detection and correction technique in cardiac SPECT imaging, *Journal of Nuclear Cardiology* **16**(4): 580–589.
URL: *http://dx.doi.org/10.1007/s12350-009-9096-7*

Baumgartner, C. F., Kolbitsch, C., Balfour, D. R., Marsden, P. K., McClelland, J. R., Rueckert, D. & King, A. P. (2014). High-resolution dynamic MR imaging of the thorax for respiratory motion correction of PET using groupwise manifold alignment, *Medical Image Analysis* **18**(7): 939–952.
URL: *http://www.sciencedirect.com/science/article/pii/S1361841514000917*

Baumgartner, C. F., Kolbitsch, C., McClelland, J. R., Rueckert, D. & King, A. P. (2017). Autoadaptive motion modelling for MR-based respiratory motion estimation, *Medical Image Analysis* **35**: 83–100.
URL: *http://www.sciencedirect.com/science/article/pii/S1361841516300822*

Beddar, A. S., Kainz, K., Briere, T. M., Tsunashima, Y., Pan, T., Prado, K., Mohan, R., Gillin, M. & Krishnan, S. (2007). Correlation between internal fiducial tumor motion and external marker motion for liver tumors imaged with 4D-CT, *International Journal of Radiation Oncology, Biology, Physics* **67**(2): 630–638.

Belkin, M. & Niyogi, P. (2003). Laplacian Eigenmaps for Dimensionality Reduction and Data Representation, *Neural Computation* **15**(6): 1373–1396.
URL: *http://dx.doi.org/10.1162/089976603321780317*

Benchetrit, G. (2000). Breathing pattern in humans: Diversity and individuality, *Respiration physiology* **122**: 123–9.

Bendriem, B., Reed, J., McCullough, K., Khan, M. R., Smith, A. M., Thomas, D. & Long, M. (2018). The continual innovation of commercial pet/ct solutions in nuclear cardiology: Siemens healthineers, *Journal of Nuclear Cardiology* **25**(4): 1400–1411.

Bertolli, O. (2018). *Data-driven methods for respiratory signal detection in positron emission tomography*, Doctoral, UCL (University College London). Conference Name: UCL (University College London) Meeting Name: UCL (University College London) Pages: 1-149 Publication Title: Doctoral thesis, UCL (University College London).
URL: *https://discovery.ucl.ac.uk/id/eprint/10046541/*

Bertolli, O., Arridge, S., Stearns, C. W., Wollenweber, S. D., Hutton, B. F. & Thielemans, K. (2016). Data driven respiratory signal detection in PET taking advantage of time-of-flight data, *2016 IEEE Nuclear Science Symposium, Medical Imaging Conference and Room-Temperature Semiconductor Detector Workshop (NSS/MIC/RTSD)*, IEEE, pp. 1–3. event-place: Strasbourg, France.
URL: *http://dx.doi.org/10.1109/nssmic.2016.8069426*

Bertolli, O., Arridge, S., Wollenweber, S. D., Stearns, C. W., Hutton, B. F. & Thielemans, K. (2017). Sign determination methods for the respiratory signal in data-driven PET gating, *Physics in Medicine and Biology* **62**(8): 3204–3220.
URL: *http://dx.doi.org/10.1088/1361-6560/aa6052*

Bertolli, O., Cuplov, V., Arridge, S., Stearns, C. W., Wollenweber, S. D., Hutton, B. F. & Thielemans, K. (2017). Detection of Lung Density Variations With Principal Component Analysis in PET, *2017 IEEE Nuclear Science Symposium and Medical Imaging Conference (NSS/MIC)*, pp. 1–3. ISSN: 2577-0829.

Bettinardi, V., De Bernardi, E., Presotto, L. & Gilardi, M. C. (2013). Motion-Tracking Hardware and Advanced Applications in PET and PET/CT, *PET Clinics* **8**(1): 11–28.

URL: *http://dx.doi.org/10.1016/j.cpet.2012.09.008*

Bettinardi, V., Picchio, M., Di Muzio, N., Gianolli, L., Gilardi, M. C. C. & Messa, C. (2010). Detection and compensation of organ/lesion motion using 4D-PET/CT respiratory gated acquisition techniques., *Radiotherapy and oncology : journal of the European Society for Therapeutic Radiology and Oncology* **96**(3): 311–316.
URL: *http://dx.doi.org/10.1016/j.radonc.2010.07.014*

Bettinardi, V., Picchio, M., Di Muzio, N. & Gilardi, M. C. (2012). Motion Management in Positron Emission Tomography/Computed Tomography for Radiation Treatment Planning, *Seminars in Nuclear Medicine* **42**(5): 289–307.
URL: *http://dx.doi.org/10.1053/j.semnuclmed.2012.04.001*

Beyer, T., Antoch, G., Blodgett, T., Freudenberg, L. F., Akhurst, T. & Mueller, S. (2003). Dual-modality PET/CT imaging: the effect of respiratory motion on combined image quality in clinical oncology, *European Journal of Nuclear Medicine and Molecular Imaging* **30**(4): 588–596.

Bloomfield, P. M., Spinks, T. J., Reed, J., Schnorr, L., Westrip, A. M., Livieratos, L., Fulton, R. & Jones, T. (2003). The design and implementation of a motion correction scheme for neurological PET, *Physics in Medicine and Biology* **48**(8): 959–978.
URL: *http://dx.doi.org/10.1088/0031-9155/48/8/301*

Blume, M., Martinez-Müller, A., Keil, A., Navab, N. & Rafecas, M. (2010). Joint reconstruction of image and motion in gated positron emission tomography, *IEEE Transactions on Medical Imaging* **29**(11): 1892–1906.

Blume, M., Navab, N. & Rafecas, M. (2012). Joint image and motion reconstruction for PET using a B-spline motion model, *Physics in Medicine and Biology* **57**(24): 8249+.
URL: *http://dx.doi.org/10.1088/0031-9155/57/24/8249*

Boucher, L., Rodrigue, S., Lecomte, R. & Bénard, F. (2004). Respiratory gating for 3-dimensional pet of the thorax: feasibility and initial results., *Journal of nuclear medicine : official publication, Society of Nuclear Medicine* **45**: 214–219.

Bousse, A., Bertolli, O., Atkinson, D., Arridge, S., Ourselin, S., Hutton, B. F. & Thielemans, K. (2016a). Maximum-likelihood joint image reconstruction and motion estimation with misaligned attenuation in TOF-PET/CT, *Physics in Medicine & Biology* **61**(3): L11–19.

Bousse, A., Bertolli, O., Atkinson, D., Arridge, S., Ourselin, S., Hutton, B. F. & Thielemans, K. (2016b). Maximum-likelihood joint image reconstruction/motion estimation in attenuation-corrected respiratory gated PET/CT using a single attenuation map, *IEEE Transactions on Medical Imaging* **35**(1): 217–228.

Bousse, A., Manber, R., Holman, B. F., Atkinson, D., Arridge, S., Ourselin, S., Hutton, B. F. & Thielemans, K. (2017). Evaluation of a direct motion estimation/correction method in respiratory-gated PET/MRI with motion-adjusted attenuation, *Medical Physics* **44**(6): 2379–2390.

Brahme, A., Nyman, P. & Skatt, B. (2008). 4D laser camera for accurate patient positioning, collision avoidance, image fusion and adaptive approaches during diagnostic and therapeutic procedures, *Medical Physics* **35**(5): 1670–1681.

Bruyant, P. P., King, M. A. & Pretorius, P. H. (2002). Correction of the respiratory motion of the heart by tracking of the center of mass of thresholded projections: a simulation study using the dynamic MCAT phantom, *IEEE Transactions on Nuclear Science* **49**(5): 2159–2166.
URL: *http://dx.doi.org/10.1109/tns.2002.803678*

Bruyant, P., Turzo, A., Bizais, Y., Cheze Le Rest, C. & Visvikis, D. (2006). A comparison of three respiratory gating methods in PET imaging for oncology, *Journal of nuclear medicine* **47**(suppl1): 183P–a.

Büther, F., Dawood, M., Stegger, L., Wübbeling, F., Schäfers, M., Schober, O. & Schäfers, K. P. (2009). List mode-driven cardiac and respiratory gating in PET., *Journal of nuclear medicine : official publication, Society of Nuclear Medicine* **50**(5): 674–681.

URL: *http://dx.doi.org/10.2967/jnumed.108.059204*

Büther, F., Jones, J., Seifert, R., Stegger, L., Schleyer, P. & Schäfers, M. (2020). Clinical Evaluation of a Data-Driven Respiratory Gating Algorithm for Whole-Body PET with Continuous Bed Motion, *Journal of Nuclear Medicine* **61**(10): 1520–1527. tex.ids= buther2020ClinicalEvaluationDataDrivena publisher: Society of Nuclear Medicine section: Physics and Instrumentation.
URL: *https://jnm.snmjournals.org/content/61/10/1520*

Buhler, P., Just, U., Will, E., Kotzerke, J. & van den Hoff, J. (2004). An Accurate Method for Correction of Head Movement in PET, *IEEE Transactions on Medical Imaging* **23**(9): 1176–1185.
URL: *http://ieeexplore.ieee.org/document/1327696/*

Bundschuh, R. A., Martínez-Moeller, A., Essler, M., Martínez, M.-J. J., Nekolla, S. G., Ziegler, S. I. & Schwaiger, M. (2007). Postacquisition detection of tumor motion in the lung and upper abdomen using list-mode PET data: a feasibility study., *Journal of nuclear medicine : official publication, Society of Nuclear Medicine* **48**(5): 758–763.
URL: *http://dx.doi.org/10.2967/jnumed.106.035279*

Callahan, J., Binns, D., Deller, T. & Hicks, R. J. (2012). Scatter Limitation to Correct for Arm Movement in PET/CT, *Clinical Nuclear Medicine* **37**(8): 786–787.
URL: *https://journals.lww.com/00003072-201208000-00017*

Carson, R. E., Barker, W. C., Liow, J.-S. & Johnson, C. A. (2003). Design of a motion-compensation osem list-mode algorithm for resolution-recovery reconstruction for the hrrt, *2003 IEEE Nuclear Science Symposium. Conference Record (IEEE Cat. No. 03CH37515)*, Vol. 5, IEEE, pp. 3281–3285.

Celicanin, Z., Auboiroux, V., Bieri, O., Petrusca, L., Santini, F., Viallon, M., Scheffler, K. & Salomir, R. (2014). Real-time method for motion-compensated MR thermometry and MRgHIFU treatment in abdominal organs, *Magnetic Resonance in Medicine* **72**(4): 1087–1095. _eprint: https://onlinelibrary.wiley.com/doi/pdf/10.1002/mrm.25017.
URL: *https://onlinelibrary.wiley.com/doi/abs/10.1002/mrm.25017*

Chan, C., Jin, X., Fung, E. K., Naganawa, M., Mulnix, T., Carson, R. E. & Liu, C. (2013). Event-by-event respiratory motion correction for PET with 3D internal-1D external motion correlation: Event-by-event respiratory motion correction for PET, *Medical Physics* **40**(11): 112507. Number: 11.
URL: *http://doi.wiley.com/10.1118/1.4826165*

Chan, C., Onofrey, J., Jian, Y., Germino, M., Papademetris, X., Carson, R. E. & Liu, C. (2018). Non-Rigid Event-by-Event Continuous Respiratory Motion Compensated List-Mode Reconstruction for PET, *IEEE Transactions on Medical Imaging* **37**(2): 504–515. Number: 2.
URL: *http://ieeexplore.ieee.org/document/8063940/*

Chang, G., Chang, T., Pan, T., Clark, J. W. & Mawlawi, O. R. (2010). Implementation of an automated respiratory amplitude gating technique for PET/CT: clinical evaluation, *Journal of Nuclear Medicine* **51**(1): 16–24.

Chun, S. Y. & Fessler, J. A. (2012). Spatial resolution properties of motion-compensated tomographic image reconstruction methods, *IEEE Transactions on Medical Imaging* **31**(7): 1413–1425.

Chun, S. Y. & Fessler, J. A. (2013). Noise properties of motion-compensated tomographic image reconstruction methods, *IEEE Transactions on Medical Imaging* **32**(2): 141–152.

Chun, S. Y., Reese, T. G., Ouyang, J., Guérin, B., Catana, C., Zhu, X., Alpert, N. M. & El Fakhri, G. (2012). MRI-Based nonrigid motion correction in simultaneous PET/MRI, *Journal of Nuclear Medicine* **53**(8): 1413–1425.

Chun, S. Y., Reese, T. G., Ouyang, J., Guerin, B., Catana, C., Zhu, X., Alpert, N. M. & Fakhri, G. E. (2012). MRI-Based Nonrigid Motion Correction in Simultaneous PET/MRI, *Journal of Nuclear Medicine* **53**(8): 1284–1291. tex.ids= chun2012MRIBasedNonrigidMotiona publisher: Society of Nuclear Medicine section: Basic Science Investigations.

URL: *http://dx.doi.org/10.2967/jnumed.111.092353*

Dawood, M., Büther, F., Lang, N., Schober, O. & Schäfers, K. P. (2007). Respiratory gating in positron emission tomography: a quantitative comparison of different gating schemes, *Medical Physics* **34**(7): 3067–3076.

Dawood, M., Buether, F., Stegger, L., Jiang, X., Schober, O., Schaefers, M. & Schaefers, K. P. (2009). Optimal number of respiratory gates in positron emission tomography: A cardiac patient study, *Medical Physics* **36**(5): 1775–1784.
URL: *http://dx.doi.org/10.1118/1.3112422*

Dawood, M., Kösters, T., Fieseler, M., Büther, F., Jiang, X., Wübbeling, F. & Schäfers, K. P. (2008). Motion correction in respiratory gated cardiac PET/CT using multi-scale optical flow, *International Conference on Medical Image Computing and Computer-Assisted Intervention*, Springer, pp. 155–162.

Dawood, M., Lang, N., Jiang, X. & Schafers, K. P. (2006). Lung motion correction on respiratory gated 3-D PET/CT images, *IEEE Transactions on Medical Imaging* **25**(4): 476–485. tex.ids= dawood2006LungMotionCorrectiona.
URL: *http://dx.doi.org/10.1109/tmi.2006.870892*

De Pierro, A. R. (1995). A modified expectation maximization algorithm for penalized likelihood estimation in emission tomography, *IEEE Transactions on Medical Imaging* **14**(1): 132–137. Conference Name: IEEE Transactions on Medical Imaging.

De Troyer, A. & Estenne, M. (1984). Coordination between rib cage muscles and diaphragm during quiet breathing in humans, *Journal of Applied Physiology* **57**(3): 899–906. Publisher: American Physiological Society.
URL: *https://journals.physiology.org/doi/abs/10.1152/jappl.1984.57.3.899*

Defrise, M., Rezaei, A. & Nuyts, J. (2012). Time-of-flight PET data determine the attenuation sinogram up to a constant, *Physics in Medicine and Biology* **57**(4): 885–899.

Didierlaurent, D., Ribes, S., Batatia, H., Jaudet, C., Dierickx, L. O., Zerdoud, S., Brillouet, S., Caselles, O. & Courbon, F. (2012). The retrospective binning method improves the consistency of phase binning in respiratory-gated PET/CT, *Physics in Medicine and Biology* **57**(23): 7829+.
URL: *http://dx.doi.org/10.1088/0031-9155/57/23/7829*

Dikaios, N. & Fryer, T. D. (2012). Registration-weighted motion correction for PET, *Medical Physics* **39**(3): 1253–1264.
URL: *http://dx.doi.org/10.1118/1.3675922*

Dikaios, N., Izquierdo-Garcia, D., Graves, M. J., Mani, V., Fayad, Z. A. & Fryer, T. D. (2012). MRI-based motion correction of thoracic PET: initial comparison of acquisition protocols and correction strategies suitable for simultaneous PET/MRI systems, *European radiology* **22**(2): 439–446.

Edwards, A. D. & Arthurs, O. J. (2011). Paediatric MRI under sedation: is it necessary? What is the evidence for the alternatives?, *Pediatric Radiology* **41**(11): 1353–1364.

Ehrhardt, J., Werner, R., Säring, D., Frenzel, T., Lu, W., Low, D. & Handels, H. (2007). An optical flow based method for improved reconstruction of 4D CT data sets acquired during free breathing, *Medical Physics* **34**(2): 711–721. _eprint: https://aapm.onlinelibrary.wiley.com/doi/pdf/10.1118/1.2431245.
URL: *https://aapm.onlinelibrary.wiley.com/doi/abs/10.1118/1.2431245*

Émond, E. C., Bousse, A., Brusaferri, L., Hutton, B. F. & Thielemans, K. (2020). Improved PET/CT respiratory motion compensation by incorporating changes in lung density, *IEEE Transactions on Radiation and Plasma Medical Sciences* **4**(5): 594–602.

Emond, E. C., Bousse, A., Machado, M., Porter, J., Erlandsson, K., Groves, A. M., Hutton, B. F. & Thielemans, K. (2019). Respiratory Motion Correction in Dynamic PET with a Single Attenuation Map, *2019 IEEE Nuclear Science Symposium and Medical Imaging Conference (NSS/MIC)*, pp. 1–3. ISSN: 2577-0829.

Ens, S., Ulrici, J., Hell, E. & Buzug, T. M. (2010). Automatic detection of patient motion in cone-beam

computed tomography, *Biomedical Imaging: From Nano to Macro, 2010 IEEE International Symposium on*, IEEE, pp. 1257–1260.
URL: *http://dx.doi.org/10.1109/isbi.2010.5490224*

Fayad, H., Gilles, M., Pan, T. & Visvikis, D. (2018). A 4D global respiratory motion model of the thorax based on CT images: A proof of concept, *Medical Physics* **45**.

Fayad, H. J., Buerger, C., Tsoumpas, C., Cheze-Le-Rest, C. & Visvikis, D. (2012). A generic respiratory motion model based on 4D MRI imaging and 2D image navigators, *2012 IEEE Nuclear Science Symposium and Medical Imaging Conference Record (NSS/MIC)*, pp. 4058–4061. ISSN: 1082-3654.

Fayad, H. J., Lamare, F., Cheze-Le Rest, C., Bettinardi, V. & Visvikis, D. (2013). Generation of 4-dimensional CT images based on 4-dimensional PET-derived motion fields, *Journal of Nuclear Medicine* **54**(4): 631–638.

Fayad, H., Odille, F., Schmidt, H., Würslin, C., Küstner, T., Felblinger, J. & Visvikis, D. (2015). The use of a generalized reconstruction by inversion of coupled systems (GRICS) approach for generic respiratory motion correction in PET/MR imaging, *Physics in Medicine & Biology* **60**(6): 2529.

Fayad, H., Pan, T., Clement, J. & Visvikis, D. (2011). Technical Note: Correlation of respiratory motion between external patient surface and internal anatomical landmarks, *Medical physics* **38**: 3157–64.

Fayad, H., Pan, T., Pradier, O. & Visvikis, D. (2012). Patient specific respiratory motion modeling using a 3D patient's external surface, *Medical Physics* **39**(6): 3386. Publisher: American Association of Physicists in Medicine.
URL: *https://www.ncbi.nlm.nih.gov/pmc/articles/PMC4032399/*

Fayad, H., Schmidt, H., Würslin, C. & Visvikis, D. (2015). Reconstruction-incorporated respiratory motion correction in clinical simultaneous PET/MR imaging for oncology applications, *Journal of Nuclear Medicine* **56**(6): 884–889.

Feng, T., Wang, J., Fung, G. & Tsui, B. (2016). Non-rigid dual respiratory and cardiac motion correction methods after, during, and before image reconstruction for 4D cardiac PET, *Physics in Medicine and Biology* **61**(1): 151–168.

Feng, T., Wang, J., Sun, Y., Zhu, W., Dong, Y. & Li, H. (2017). Self-Gating: An Adaptive Center-of-mass Approach for Respiratory Gating in PET, *IEEE Transactions on Medical Imaging* p. 1. tex.ids= feng2018SelfGatingAdaptiveCenterofMass conferenceName: IEEE Transactions on Medical Imaging.
URL: *http://dx.doi.org/10.1109/tmi.2017.2783739*

Feng, T., Yang, G., Li, H., Shi, H., Cherry, S., Badawi, R. & Dong, Y. (2020). Data-driven respiratory gating for the uEXPLORER with fast dynamics, *Journal of Nuclear Medicine* **61**(supplement 1): 368–368. Publisher: Society of Nuclear Medicine Section: Physics, Instrumentation & Data Sciences.

Fieseler, M., Gigengack, F., Jiang, X. & Schäfers, K. P. (2014). Motion Correction of Whole-Body PET Data with a Joint PET-MRI Registration Functional, *Biomed Eng Online* **13**(Suppl 1): S2.
URL: *https://www.ncbi.nlm.nih.gov/pmc/articles/PMC4108932/*

Fischer, R. W., Botnar, R. M., Nehrke, K., Boesiger, P., Manning, W. J. & Peters, D. C. (2006). Analysis of residual coronary artery motion for breath hold and navigator approaches using real-time coronary MRI, *Magnetic Resonance in Medicine* **55**(3): 612–618. _eprint: https://onlinelibrary.wiley.com/doi/pdf/10.1002/mrm.20809.
URL: *https://onlinelibrary.wiley.com/doi/abs/10.1002/mrm.20809*

Fulton, R. (2001). *Correction for patient head movement in emission tomography*, PhD Thesis, University of Technology, Sydney, Department of applied physics, Sydney.

Gaede, S., Carnes, G., Yu, E., Van Dyk, J., Battista, J. & Lee, T.-Y. (2009). The use of CT density changes at internal tissue interfaces to correlate internal organ motion with an external surrogate, *Physics in Medicine and Biology* **54**(2): 259–273.

Gallezot, J.-D., Lu, Y., Naganawa, M. & Carson, R. E. (2018). Parametric Imaging With PET and

SPECT, *IEEE Transactions on Radiation and Plasma Medical Sciences* **4**(1): 1–23. Number: 1.
URL: *https://ieeexplore.ieee.org/document/8680675/*

Geimer, T., Unberath, M., Birlutiu, A., Taubmann, O., Wölfelschneider, J., Bert, C. & Maier, A. (2017). A kernel-based framework for intra-fractional respiratory motion estimation in radiation therapy, *2017 IEEE 14th International Symposium on Biomedical Imaging (ISBI 2017)*, pp. 1036–1039. ISSN: 1945-8452.

Germino, M., Sinusas, A. J., Liu, C. & Carson, R. E. (2014). Direct EM reconstruction of kinetic parameters from list-mode cardiac PET, *2014 IEEE Nuclear Science Symposium and Medical Imaging Conference (NSS/MIC)*, IEEE, Seattle, WA, USA, pp. 1–4.
URL: *http://ieeexplore.ieee.org/document/7430812/*

Gierga, D., Brewer, J., Sharp, G., Betke, M., Willett, C. & Chen, G. (2005). The correlation between internal and external markers for abdominal tumors: Implications for respiratory gating, *International Journal of Radiation Oncology*Biology*Physics* **61**(5): 1551–1558.
URL: *http://dx.doi.org/10.1016/j.ijrobp.2004.12.013*

Gigengack, F., Ruthotto, L., Burger, M., Wolters, C. H., Jiang, X. & Schäfers, K. P. (2012). Motion correction in dual gated cardiac PET using mass-preserving image registration, *IEEE transactions on medical imaging* **31**(3): 698–712.

Gilles, M., Fayad, H., Miglierini, P., Clement, J. F., Scheib, S., Cozzi, L., Bert, J., Boussion, N., Schick, U., Pradier, O. & Visvikis, D. (2016). Patient positioning in radiotherapy based on surface imaging using time of flight cameras, *Medical Physics* **43**(8): 4833.

Gillman, A., Smith, J., Thomas, P., Rose, S. & Dowson, N. (2017). PET motion correction in context of integrated PET/MR: Current techniques, limitations, and future projections, *Medical Physics* **44**(12): e430–e445.

Ginn, J. S., Ruan, D., Low, D. A. & Lamb, J. M. (2019). Multislice motion modeling for MRI-guided radiotherapy gating, *Medical Physics* **46**(2): 465–474. _eprint: https://aapm.onlinelibrary.wiley.com/doi/pdf/10.1002/mp.13350.
URL: *https://aapm.onlinelibrary.wiley.com/doi/abs/10.1002/mp.13350*

González, R. G., Schaefer, P. W., Buonanno, F. S., Schwamm, L. H., Budzik, R. F., Rordorf, G., Wang, B., Sorensen, A. G. & Koroshetz, W. J. (1999). Diffusion-weighted MR imaging: diagnostic accuracy in patients imaged within 6 hours of stroke symptom onset, *Radiology* **210**(1): 155–162.

Grimm, R., Fürst, S., Dregely, I., Forman, C., Hutter, J. M., Ziegler, S. I., Nekolla, S., Kiefer, B., Schwaiger, M., Hornegger, J. & Block, T. (2013). Self-gated Radial MRI for Respiratory Motion Compensation on Hybrid PET/MR Systems, *in* K. Mori, I. Sakuma, Y. Sato, C. Barillot & N. Navab (eds), *Medical Image Computing and Computer-Assisted Intervention – MICCAI 2013*, Lecture Notes in Computer Science, Springer, Berlin, Heidelberg, pp. 17–24.

Guérin, B., Cho, S., Chun, S. Y., Zhu, X., Alpert, N. M., El Fakhri, G., Reese, T. & Catana, C. (2011). Nonrigid PET motion compensation in the lower abdomen using simultaneous tagged-MRI and PET imaging, *Medical Physics* **38**(6Part1): 3025–3038.

Hamill, J. J., Meier, J. G., Betancourt Cuellar, S. L., Sabloff, B., Erasmus, J. J. & Mawlawi, O. (2020). Improved Alignment of PET and CT Images in Whole-Body PET/CT in Cases of Respiratory Motion During CT, *Journal of Nuclear Medicine: Official Publication, Society of Nuclear Medicine* **61**(9): 1376–1380.

He, J., O'Keefe, G. J., Gong, S. J., Jones, G., Saunder, T., Scott, A. M. & Geso, M. (2008). A Novel Method for Respiratory Motion Gated With Geometric Sensitivity of the Scanner in 3D PET, *IEEE Transactions on Nuclear Science* **55**(5): 2557–2565.
URL: *http://dx.doi.org/10.1109/tns.2008.2001187*

Heß, M., Büther, F., Gigengack, F., Dawood, M. & Schäfers, K. P. (2015). A dual-kinect approach to determine torso surface motion for respiratory motion correction in PET, *Medical Physics* **42**(5): 2276–2286.

Hong, I., Jones, J. & Casey, M. (2014). Ultrafast elastic motion correction via motion deblurring, *2014*

IEEE Nuclear Science Symposium and Medical Imaging Conference (NSS/MIC), IEEE, pp. 1–2.

Huang, T.-C., Chou, K.-T., Wang, Y.-C. & Zhang, G. (2014). Motion freeze for respiration motion correction in PET/CT: a preliminary investigation with lung cancer patient data, *BioMed Research International* **2014**: 167491.

Hunter, C. R. R. N., Klein, R., Beanlands, R. S. & deKemp, R. A. (2016). Patient motion effects on the quantification of regional myocardial blood flow with dynamic PET imaging, *Medical Physics* **43**(4): 1829.

Hwang, D., Kim, K. Y., Kang, S. K., Seo, S., Paeng, J. C., Lee, D. S. & Lee, J. S. (2018). Improving the Accuracy of Simultaneously Reconstructed Activity and Attenuation Maps Using Deep Learning, *Journal of Nuclear Medicine: Official Publication, Society of Nuclear Medicine* **59**(10): 1624–1629.

Ionascu, D., Jiang, S. B., Nishioka, S., Shirato, H. & Berbeco, R. I. (2007). Internal-external correlation investigations of respiratory induced motion of lung tumors, *Medical Physics* **34**(10): 3893–3903.

Jacobson, M. W. (2006). *Approaches to Motion-Corrected PET Image Reconstruction from Respiratory Gated Projection Data*, PhD thesis, The University of Michigan, Ann Arbor, USA.

Jacobson, M. W. & Fessler, J. (2006). Joint Estimation of Respiratory Motion and Activity in 4D PET Using CT Side Information, *3rd IEEE International Symposium on Biomedical Imaging: Macro to Nano, 2006.*, IEEE, Arlington, Virginia, USA, pp. 275–278.
URL: *http://dx.doi.org/10.1109/isbi.2006.1624906*

Jacobson, M. W. & Fessler, J. A. (2003a). Joint estimation of image and deformation parameters in motion-corrected PET, *2003 IEEE Nuclear Science Symposium. Conference Record*, IEEE, Portland, OR, USA, pp. 3290–3294.
URL: *http://dx.doi.org/10.1109/nssmic.2003.1352599*

Jacobson, M. W. & Fessler, J. A. (2003b). Joint estimation of image and deformation parameters in motion-corrected PET, *IEEE Science Symposium Conference Record*, Vol. 5, pp. 3290–3294.

Jani, S. S., Robinson, C. G., Dahlbom, M., White, B. M., Thomas, D. H., Gaudio, S., Low, D. A. & Lamb, J. M. (2013). A comparison of amplitude-based and phase-based positron emission tomography gating algorithms for segmentation of internal target volumes of tumors subject to respiratory motion, *International Journal of Radiation Oncology, Biology, Physics* **87**(3): 562–569.

Jiao, J., Bousse, A., Thielemans, K., Burgos, N., Weston, P., Markiewicz, P., Schott, J., Atkinson, D., Arridge, S., Hutton, B. F. & Ourselin, S. (2017). Direct parametric reconstruction with joint motion estimation/correction for dynamic brain PET data, *IEEE Transactions on Medical Imaging* **36**(1): 203–213.

Karakatsanis, N. A., Tsoumpas, C. & Zaidi, H. (2017). Quantitative PET image reconstruction employing nested expectation-maximization deconvolution for motion compensation, *Computerized Medical Imaging and Graphics* **60**: 11–21.
URL: *https://linkinghub.elsevier.com/retrieve/pii/S0895611116301045*

Kesner, A. L. & Kuntner, C. (2010). A new fast and fully automated software based algorithm for extracting respiratory signal from raw PET data and its comparison to other methods, *Medical Physics* **37**(10): 5550+.
URL: *http://dx.doi.org/10.1118/1.3483784*

Kesner, A. L., Schleyer, P. J., Büther, F., Walter, M. A., Schäfers, K. P. & Koo, P. J. (2014). On transcending the impasse of respiratory motion correction applications in routine clinical imaging – a consideration of a fully automated data driven motion control framework, *EJNMMI Physics* **1**(1): 8–11.
URL: *http://dx.doi.org/10.1186/2197-7364-1-8*

Kinahan, P., MacDonald, L., Ng, L., Alessio, A., Segars, P., Tsui, B. & Pathak, S. (2006). Compensating for patient respiration in PET/CT imaging with the registered and summed phases (RASP) procedure, *3rd IEEE International Symposium on Biomedical Imaging: Macro to Nano, 2006.*, IEEE, pp. 1104–1107. event-place: Arlington, Virginia, USA.

URL: *http://dx.doi.org/10.1109/isbi.2006.1625115*

King, A. P., Tsoumpas, C., Buerger, C., Schulz, V., Marsden, P. & Schaeffter, T. (2011). Real-time respiratory motion correction for simultaneous PET-MR using an MR-derived motion model, *2011 IEEE Nuclear Science Symposium Conference Record*, IEEE, pp. 3589–3594.

Kitamura, Y., Baba, S., Isoda, T., Maruoka, Y., Kawanami, S., Himuro, K., Sasaki, M. & Honda, H. (2017). The Efficiency of Respiratory-gated 18F-FDG PET/CT in Lung Adenocarcinoma: Amplitude-gating Versus Phase-gating Methods, *Asia Oceania Journal of Nuclear Medicine & Biology* **5**(1): 30–36.

Klein, G. J., Reutter, B. W. & Huesman, R. H. (1996). Non-rigid summing of gated PET via optical flow, *Nuclear Science Symposium, 1996. Conference Record., 1996 IEEE*, Vol. 2, Anaheim, CA, USA, pp. 1339–1342.
URL: *http://dx.doi.org/10.1109/nssmic.1996.591692*

Klein, G., Reutter, B., Botvinick, E., Budinger, T. & Huesman, R. (2001). Fine-scale motion detection using intrinsic list mode PET information, *Workshop on Mathematical Methods in Biomedical Image Analysis*, Vol. 0, IEEE Comput. Soc, Los Alamitos, CA, USA, pp. 71–78. event-place: Kauai, HI, USA.
URL: *http://dx.doi.org/10.1109/mmbia.2001.991701*

Klén, R., Noponen, T., Koikkalainen, J., Lötjönen, J., Thielemans, K., Hoppela, E., Sipilä, H., Teräs, M. & Knuuti, J. (2016). Evaluation of motion-correction methods for dual-gated cardiac positron emission tomography/computed tomography imaging, *Nuclear Medicine Communications* **37**(9): 956–968.

Kolbitsch, C., Ahlman, M. A., Davies-Venn, C., Evers, R., Hansen, M., Peressutti, D., Marsden, P., Kellman, P., Bluemke, D. A. & Schaeffter, T. (2017). Cardiac and Respiratory Motion Correction for Simultaneous Cardiac PET/MR, *Journal of Nuclear Medicine: Official Publication, Society of Nuclear Medicine* **58**(5): 846–852.

Kolbitsch, C., Neji, R., Fenchel, M., Schuh, A., Mallia, A., Marsden, P. & Schaeffter, T. (2018). Joint cardiac and respiratory motion estimation for motion-corrected cardiac PET-MR, *Physics in Medicine and Biology* **64**(1): 015007.

Kotasidis, F. A., Matthews, J. C., Angelis, G. I., Markiewicz, P. J., Lionheart, W. R. & Reader, A. J. (2011). Impact of erroneous kinetic model formulation in Direct 4D image reconstruction, *2011 IEEE Nuclear Science Symposium Conference Record*, IEEE, Valencia, Spain, pp. 2366–2367.
URL: *http://ieeexplore.ieee.org/document/6153881/*

Kotasidis, F. A., Matthews, J. C., Reader, A. J., Angelis, G. I. & Zaidi, H. (2014). Application of adaptive kinetic modelling for bias propagation reduction in direct 4D image reconstruction, *Physics in Medicine and Biology* **59**(20): 6061–6084. Number: 20.
URL: *https://iopscience.iop.org/article/10.1088/0031-9155/59/20/6061*

Küstner, T., Armanious, K., Yang, J., Yang, B., Schick, F. & Gatidis, S. (2019). Retrospective correction of motion-affected MR images using deep learning frameworks, *Magnetic resonance in medicine* .

Küstner, T., Schwartz, M., Martirosian, P., Gatidis, S., Seith, F., Gilliam, C., Blu, T., Fayad, H., Visvikis, D., Schick, F., Yang, B., Schmidt, H. & Schwenzer, N. F. (2017). MR-based respiratory and cardiac motion correction for PET imaging., *Medical image analysis* **42**: 129–144.
URL: *http://view.ncbi.nlm.nih.gov/pubmed/28800546*

Küstner, T., Schwartz, M., Martirosian, P., Gatidis, S., Seith, F., Gilliam, C., Blu, T., Fayad, H., Visvikis, D., Schick, F. et al. (2017). Mr-based respiratory and cardiac motion correction for PET imaging, *Medical Image Analysis* **42**: 129–144.

Kyme, A., Se, S., Meikle, S., Angelis, G., Ryder, W., Popovic, K., Yatigammana, D. & Fulton, R. (2014). Markerless motion tracking of awake animals in positron emission tomography, *IEEE transactions on medical imaging* **33**(11): 2180–2190.

Kyme, A. Z. & Fulton, R. R. (2021). Motion estimation and correction in SPECT, PET and CT, *Phys. Med. Biol.* .

URL: *http://iopscience.iop.org/article/10.1088/1361-6560/ac093b*

Kyme, A. Z., Hutton, B. F., Hatton, R. L., Skerrett, D. W. & Barnden, L. R. (2003). Practical aspects of a data-driven motion correction approach for brain SPECT, *Medical Imaging, IEEE Transactions on* **22**(6): 722–729.
URL: *http://dx.doi.org/10.1109/tmi.2003.814790*

Lamare, F., Carbayo, M. J. L., Cresson, T., Kontaxakis, G., Santos, A., Cheze-Le Rest, C., Reader, A. J. & Visvikis, D. (2007). List-mode-based reconstruction for respiratory motion correction in PET using non-rigid body transformations, *Physics in Medicine & Biology* **52**: 5187–5204.

Lamare, F., Cresson, T., Savean, J., Cheze-Le Rest, C., Reader, A. J. & Visvikis, D. (2007). Respiratory motion correction for PET oncology applications using affine transformation of list mode data, *Physics in Medicine & Biology* **52**(1): 121–140.

Lamare, F., Lemaitre, A., Fernandez, P., Rimoldi, O. & Visvikis, D. (2014). Evaluation of respiratory and cardiac motion correction schemes in dual gated pet/ct cardiac imaging, *Medical physics* **41**(7): 072504.

Lang, N., Dawood, M., Büther, F., Schober, O., Schäfers, M. & Schäfers, K. (2006). Organ movement reduction in PET/CT using dual-gated list-mode acquisition, *Zeitschrift Fur Medizinische Physik* **16**(1): 93–100.

Lange, K. & Carson, R. (1984). EM reconstruction algorithms for emission and transmission tomography, *Journal of Computer Assisted Tomography* **8**(2): 306–316.

Lee, K. J. & Barber, D. C. (1999). Use of forward projection to correct patient motion during SPECT imaging, *Physics in Medicine and Biology* **43**(1): 171+.
URL: *http://dx.doi.org/10.1088/0031-9155/43/1/011*

Li, T., Thorndyke, B., Schreibmann, E., Yang, Y. & Xing, L. (2006). Model-based image reconstruction for four-dimensional pet, *Medical physics* **33**(5): 1288–1298.

Li, T., Zhang, M., Qi, W., Asma, E. & Qi, J. (2020). Motion correction of respiratory-gated PET images using deep learning based image registration framework, *Physics in Medicine and Biology* **65**(15): 155003.

Liberini, V., Kotasidis, F., Treyer, V., Messerli, M., Orita, E., Engel-Bicik, I., Siebenhüner, A. & Huellner, M. W. (2021). Impact of PET data driven respiratory motion correction and BSREM reconstruction of 68 Ga-DOTATATE PET/CT for differentiating neuroendocrine tumors (NET) and intrapancreatic accessory spleens (IPAS), *Scientific Reports* **11**(1): 2273. Number: 1 Publisher: Nature Publishing Group.
URL: *https://www.nature.com/articles/s41598-020-80855-4*

Liu, C., Alessio, A. M. & Kinahan, P. E. (2011). Respiratory motion correction for quantitative PET/CT using all detected events with internal—external motion correlation, *Medical Physics* **38**(5): 2715+.
URL: *http://dx.doi.org/10.1118/1.3582692*

Liu, C., Alessio, A., Pierce, L., Thielemans, K., Wollenweber, S., Ganin, A. & Kinahan, P. (2010). Quiescent period respiratory gating for PET/CT, *Medical Physics* **37**(9): 5037. tex.ids: liu2010QuiescentPeriodRespiratory publisher: American Association of Physicists in Medicine.
URL: *https://www.ncbi.nlm.nih.gov/pmc/articles/PMC2945743/*

Liu, C., Pierce, L. A., Alessio, A. M. & Kinahan, P. E. (2009). The impact of respiratory motion on tumor quantification and delineation in static PET/CT imaging, *Physics in Medicine and Biology* **54**(24): 7345–7362.

Livieratos, L., Stegger, L., Bloomfield, P. M., Schafers, K., Bailey, D. L. & Camici, P. G. (2005a). Rigid-body transformation of list-mode projection data for respiratory motion correction in cardiac pet, *Physics in Medicine & Biology* **50**(14): 3313.

Livieratos, L., Stegger, L., Bloomfield, P. M., Schafers, K., Bailey, D. L. & Camici, P. G. (2005b). Rigid-body transformation of list-mode projection data for respiratory motion correction in cardiac PET, *Physics in Medicine and Biology* **50**(14): 3313–3322.

Livieratos, L., Stegger, L., Bloomfield, P. M., Schafers, K., Bailey, D. L. & Camici, P. G. (2005c). Rigid-

body transformation of list-mode projection data for respiratory motion correction in cardiac PET, *Physics in Medicine and Biology* **50**(14): 3313–3322.
URL: *http://dx.doi.org/10.1088/0031-9155/50/14/008*

Lodge, M. A., Mhlanga, J. C., Cho, S. Y. & Wahl, R. L. (2011). Effect of Patient Arm Motion in Whole-Body PET/CT, *Journal of Nuclear Medicine* **52**(12): 1891–1897. Publisher: Society of Nuclear Medicine Section: Brief Communications.
URL: *https://jnm.snmjournals.org/content/52/12/1891*

Lu, Y., Fontaine, K., Mulnix, T., Onofrey, J. A., Ren, S., Panin, V., Jones, J., Casey, M. E., Barnett, R., Kench, P., Fulton, R., Carson, R. E. & Liu, C. (2018). Respiratory Motion Compensation for PET/CT with Motion Information Derived from Matched Attenuation-Corrected Gated PET Data, *Journal of Nuclear Medicine: Official Publication, Society of Nuclear Medicine* **59**(9): 1480–1486.

Lu, Y., Gallezot, J.-D., Naganawa, M., Ren, S., Fontaine, K., Wu, J., Onofrey, J. A., Toyonaga, T., Boutagy, N., Mulnix, T., Panin, V. Y., Casey, M. E., Carson, R. E. & Liu, C. (2019). Data-driven voluntary body motion detection and non-rigid event-by-event correction for static and dynamic PET, *Physics in Medicine & Biology* **64**(6): 065002. Number: 6.
URL: *https://iopscience.iop.org/article/10.1088/1361-6560/ab02c2*

Lupi, A., Zaroccolo, M., Salgarello, M., Malfatti, V. & Zanco, P. (2009). The effect of 18F-FDG-PET/CT respiratory gating on detected metabolic activity in lung lesions, *Annals of Nuclear Medicine* **23**(2): 191–196.
URL: *http://dx.doi.org/10.1007/s12149-008-0225-1*

Manber, R., Thielemans, K., Hutton, B. F., Barnes, A., Ourselin, S., Arridge, S., O'Meara, C., Wan, S. & Atkinson, D. (2015). Practical PET respiratory motion correction in clinical PET/MR, *Journal of Nuclear Medicine* **56**(6): 890–896.

Manber, R., Thielemans, K., Hutton, B. F., Wan, S., Fraioli, F., Barnes, A., Ourselin, S., Arridge, S. & Atkinson, D. (2018). Clinical impact of respiratory motion correction in simultaneous PET/MR, using a joint PET/MR predictive motion model, *Journal of Nuclear Medicine* **59**(9): 1467–1473.

Manber, R., Thielemans, K., Hutton, B. F., Wan, S., McClelland, J., Barnes, A., Arridge, S., Ourselin, S. & Atkinson, D. (2016). Joint PET-MR respiratory motion models for clinical PET motion correction, *Physics in Medicine & Biology* **61**(17): 6515–6530.

Manjeshwar, R., Xiaodong, T., Asma, E. & Thielemans, K. (2006). Motion compensated image reconstruction of respiratory gated PET/CT, *3rd IEEE International Symposium on Biomedical Imaging: Nano to Macro, 2006* pp. 674–677.

Manke, D., Nehrke, K. & Boernert, P. (2003). Novel prospective respiratory motion correction approach for free-breathing coronary MR angiography using a patient-adapted affine motion model, *Magnetic Resonance in Medicine* **50**(1): 122–131. _eprint: https://onlinelibrary.wiley.com/doi/pdf/10.1002/mrm.10483.
URL: *https://onlinelibrary.wiley.com/doi/abs/10.1002/mrm.10483*

McClelland, J. R., Blackall, J. M., Tarte, S., Chandler, A. C., Hughes, S., Ahmad, S., Landau, D. B. & Hawkes, D. J. (2006). A continuous 4D motion model from multiple respiratory cycles for use in lung radiotherapy, *Medical Physics* **33**(9): 3348–3358. _eprint: https://aapm.onlinelibrary.wiley.com/doi/pdf/10.1118/1.2222079.
URL: *https://aapm.onlinelibrary.wiley.com/doi/abs/10.1118/1.2222079*

McClelland, J. R., Hawkes, D. J., Schaeffter, T. & King, A. P. (2013). Respiratory motion models: a review, *Medical Image Analysis* **17**(1): 19–42.

McClelland, J. R., Hughes, S., Modat, M., Qureshi, A., Ahmad, S., Landau, D. B., Ourselin, S. & Hawkes, D. J. (2010). Inter-fraction variations in respiratory motion models, *Physics in Medicine and Biology* **56**(1): 251–272. Publisher: IOP Publishing.
URL: *https://doi.org/10.1088%2F0031-9155%2F56%2F1%2F015*

McClelland, J. R., Modat, M., Arridge, S., Grimes, H., D'Souza, D., Thomas, D., Connell, D. O., Low, D. A., Kaza, E., Collins, D. J., Leach, M. O. & Hawkes, D. J. (2017). A generalized

framework unifying image registration and respiratory motion models and incorporating image reconstruction, for partial image data or full images, *Physics in Medicine and Biology* **62**(11): 4273. Publisher: IOP Publishing.
URL: *https://www.ncbi.nlm.nih.gov/pmc/articles/PMC5763581/*

McQuaid, S. J., Lambrou, T., Cunningham, V. J., Bettinardi, V., Gilardi, M. C. & Hutton, B. F. (2009). The Application of a Statistical Shape Model to Diaphragm Tracking in Respiratory-Gated Cardiac PET Images, *Proceedings of the IEEE* **97**(12): 2039–2052.
URL: *http://dx.doi.org/10.1109/jproc.2009.2031844*

McQuaid, S. J., Lambrou, T. & Hutton, B. F. (2011). A novel method for incorporating respiratory-matched attenuation correction in the motion correction of cardiac PET–CT studies, *Physics in Medicine and Biology* **56**(10): 2903–2915.
URL: *http://dx.doi.org/10.1088/0031-9155/56/10/002*

Meier, J. G., Einstein, S. A., Diab, R. H., Erasmus, L. J., Xu, G. & Mawlawi, O. R. (2019). Impact of free-breathing CT on quantitative measurements of static and quiescent period-gated PET images, *Physics in Medicine & Biology* **64**(10): 105013.

Menke, M., Atkins, M. S. & Buckley, K. R. (1996). Compensation methods for head motion detected during PET imaging, *Nuclear Science, IEEE Transactions on* **43**(1): 310–317.
URL: *http://dx.doi.org/10.1109/23.485971*

Moore, C. C., McVeigh, E. R. & Zerhouni, E. A. (2000). Quantitative tagged magnetic resonance imaging of the normal human left ventricle, *Topics in Magnetic Resonance Imaging* **11**(6): 359–371.

Mourik, J. E. M., Lubberink, M., Velden, F. H. P., Lammertsma, A. A. & Boellaard, R. (2009). Off-line motion correction methods for multi-frame PET data, *European Journal of Nuclear Medicine and Molecular Imaging* **36**(12): 2002–2013.
URL: *http://dx.doi.org/10.1007/s00259-009-1193-y*

Munoz, C., Kolbitsch, C., Reader, A., Marsden, P., Schaeffter, T. & Prieto, C. (2016). MR-Based Cardiac and Respiratory Motion-Compensation Techniques for PET-MR Imaging, *PET Clinics* **11**.

Munoz, C., Neji, R., Kunze, K. P., Nekolla, S. G., Botnar, R. M. & Prieto, C. (2019). Respiratory- and cardiac motion-corrected simultaneous whole-heart PET and dual phase coronary MR angiography, *Magnetic Resonance in Medicine* **81**(3): 1671–1684.

Nehmeh, S. A. & Erdi, Y. E. (2008). Respiratory motion in positron emission tomography/computed tomography: a review, *Seminars in Nuclear Medicine* **38**(3): 167–176.

Nehmeh, S. A., Erdi, Y. E., Ling, C. C., Rosenzweig, K. E., Squire, O. D., Braban, L. E., Ford, E., Sidhu, K., Mageras, G. S., Larson, S. M. & Humm, J. L. (2002). Effect of respiratory gating on reducing lung motion artifacts in PET imaging of lung cancer, *Medical Physics* **29**(3): 366–371.

Nehmeh, S. A., Erdi, Y. E., Meirelles, G. S., Squire, O., Larson, S. M., Humm, J. L. & Schoder, H. (2007). Deep-Inspiration Breath-Hold PET/CT of the Thorax, *J Nucl Med* **48**(1): 22–26.
URL: *http://jnm.snmjournals.org/cgi/content/abstract/48/1/22*

Nehmeh, S. A., Erdi, Y. E., Pan, T., Pevsner, A., Rosenzweig, K. E., Yorke, E., Mageras, G. S., Schoder, H., Vernon, P., Squire, O., Mostafavi, H., Larson, S. M. & Humm, J. L. (2004). Four-dimensional (4D) PET/CT imaging of the thorax, *Medical Physics* **31**(12): 3179–3186.

Nehmeh, S. A., Erdi, Y. E., Pan, T., Yorke, E., Mageras, G. S., Rosenzweig, K. E., Schoder, H., Mostafavi, H., Squire, O., Pevsner, A., Larson, S. M. & Humm, J. L. (2004). Quantitation of respiratory motion during 4D-PET/CT acquisition, *Medical Physics* **31**(6): 1333–1338.

Nehmeh, S. A., Erdi, Y. E., Rosenzweig, K. E., Schoder, H., Larson, S. M., Squire, O. D. & Humm, J. L. (2003). Reduction of respiratory motion artifacts in PET imaging of lung cancer by respiratory correlated dynamic PET: methodology and comparison with respiratory gated PET, *Journal of Nuclear Medicine: Official Publication, Society of Nuclear Medicine* **44**(10): 1644–1648.

Odille, F., Uribe, S., Batchelor, P. G., Prieto, C., Schaeffter, T. & Atkinson, D. (2010). Model-based reconstruction for cardiac cine MRI without ECG or

breath holding, *Magnetic Resonance in Medicine* **63**(5): 1247–1257. _eprint: https://onlinelibrary.wiley.com/doi/pdf/10.1002/mrm.22312.
URL: *https://onlinelibrary.wiley.com/doi/abs/10.1002/mrm.22312*

Odille, F., Vuissoz, P.-A., Marie, P.-Y. & Felblinger, J. (2008). Generalized Reconstruction by Inversion of Coupled Systems (GRICS) applied to free-breathing MRI, *Magnetic Resonance in Medicine* **60**(1): 146–157. _eprint: https://onlinelibrary.wiley.com/doi/pdf/10.1002/mrm.21623.
URL: *https://onlinelibrary.wiley.com/doi/abs/10.1002/mrm.21623*

Osman, M. M., Cohade, C., Nakamoto, Y. & Wahl, R. L. (2003). Respiratory motion artifacts on PET emission images obtained using CT attenuation correction on PET-CT, *European Journal of Nuclear Medicine and Molecular Imaging* **30**(4): 603–606.

Ozhasoglu, C. & Murphy, M. (2002). Issues in respiratory motion compensation during external-beam radiotherapy, *International Journal of Radiation OncologyBiologyPhysics* **52**(5): 1389–1399.
URL: *http://dx.doi.org/10.1016/s0360-3016(01)02789-4*

Pan, T., Lee, T.-Y., Rietzel, E. & Chen, G. T. Y. (2004). 4D-CT imaging of a volume influenced by respiratory motion on multi-slice CT, *Medical Physics* **31**(2): 333–340.

Pan, T., Mawlawi, O., Luo, D., Liu, H. H., Chi, P.-C. M., Mar, M. V., Gladish, G., Truong, M., Erasmus, J., Liao, Z. & Macapinlac, H. A. (2006). Attenuation correction of PET cardiac data with low-dose average CT in PET/CT, *Medical Physics* **33**(10): 3931–3938.

Panin, V. Y., Aykac, M. & Casey, M. E. (2013). Simultaneous reconstruction of emission activity and attenuation coefficient distribution from TOF data, acquired with external transmission source, *Physics in Medicine and Biology* **58**(11): 3649–3669.

Pearson, K. (1901). On lines and planes of closest fit to systems of points in space, *Philosophical Magazine* **2**(6): 559–572.

Pellot-Barakat, C., Ivanovic, M., Herment, A., Erlandsson, K. & Shelton, D. K. (2001). Detection of motion in hybrid PET/SPECT imaging based on the correlation of partial sinograms, *IEEE Transactions on Medical Imaging* **20**(10): 1072–1083.
URL: *http://dx.doi.org/10.1109/42.959304*

Peressutti, D., Penney, G., Kolbitsch, C. & King, A. (2013). Personalising cross-population respiratory motion models using anatomical features, *Proceedings of the 17th Conference on Medical Image Understanding and Analysis*.

Petibon, Y., El Fakhri, G., Nezafat, R., Johnson, N., Brady, T. & Ouyang, J. (2014). Towards coronary plaque imaging using simultaneous PET-MR: a simulation study, *Physics in Medicine & Biology* **59**: 1203–1222.

Petibon, Y., Sun, T., Han, P. K., Ma, C., Fakhri, G. E. & Ouyang, J. (2019). MR-based cardiac and respiratory motion correction of PET: application to static and dynamic cardiac 18F-FDG imaging, *Physics in Medicine and Biology* **64**(19): 195009.

Picard, Y. & Thompson, C. (1997). Motion correction of PET images using multiple acquisition frames, *IEEE Transactions on Medical Imaging* **16**(2): 137–144.
URL: *http://ieeexplore.ieee.org/document/563659/*

Piccinelli, M., Votaw, J. R. & Garcia, E. V. (2018). Motion Correction and Its Impact on Absolute Myocardial Blood Flow Measures with PET, *Current Cardiology Reports* **20**(5): 34. Number: 5.
URL: *http://link.springer.com/10.1007/s11886-018-0977-8*

Polycarpou, I., Soultanidis, G. & Tsoumpas, C. (2021). Synergistic motion compensation strategies for positron emission tomography when acquired simultaneously with magnetic resonance imaging, *Phil Trans Roy Soc A* **379**(2204): 20200207. tex.ids= polycarpou2021SynergisticMotionCompensationa publisher: Royal Society.
URL: *https://royalsocietypublishing.org/doi/10.1098/rsta.2020.0207*

Polycarpou, I., Tsoumpas, C. & Marsden, P. K. (2012). Analysis and comparison of two methods for motion correction in PET imaging, *Medical Physics* **39**(10): 6474–6483. _eprint: https://aapm.onlinelibrary.wiley.com/doi/pdf/10.1118/1.4754586.

URL: *https://aapm.onlinelibrary.wiley.com/doi/abs/10.1118/1.4754586*

Qi, J. & Huesman, R. H. (2002). List mode reconstruction for PET with motion compensation: a simulation study, *Proceedings IEEE International Symposium on Biomedical Imaging*, IEEE, pp. 413–416.

Qi, J. & Huesman, R. H. (2006). Penalized maximum-likelihood image reconstruction for lesion detection, *Physics in Medicine and Biology* **51**(16): 4017–4029.
URL: *http://dx.doi.org/10.1088/0031-9155/51/16/009*

Qiao, F., Pan, T., Clark Jr, J. W. & Mawlawi, O. R. (2006). A motion-incorporated reconstruction method for gated PET studies, *Physics in Medicine & Biology* **51**(15): 3769.

Rahmim, A. (2005). Advanced Motion Correction Methods in PET, *Iranian Journal of Nuclear Medicine* **13**(24): 1–17.

Rahmim, A., Bloomfield, P., Houle, S., Lenox, M., Michel, C., Buckley, K. R., Ruth, T. J. & Sossi, V. (2004). Motion compensation in histogram-mode and list-mode EM reconstructions: beyond the event-driven approach, *IEEE Transactions on Nuclear Science* **51**(5): 2588–2596.

Rahmim, A., Rousset, O. & Zaidi, H. (2007). Strategies for Motion Tracking and Correction in PET, *PET clinics* **2**(2): 251–266.

Rahmim, A., Tang, J. & Zaidi, H. (2009). Four-dimensional (4D) image reconstruction strategies in dynamic PET: Beyond conventional independent frame reconstruction: Four-dimensional PET imaging, *Medical Physics* **36**(8): 3654–3670. Number: 8.
URL: *http://doi.wiley.com/10.1118/1.3160108*

Reader, A. J. & Verhaeghe, J. (2014). 4D image reconstruction for emission tomography, *Physics in Medicine and Biology* **59**(22): R371–R418. Number: 22.
URL: *https://iopscience.iop.org/article/10.1088/0031-9155/59/22/R371*

Ren, S., Jin, X., Chan, C., Jian, Y., Mulnix, T., Liu, C. & Carson, R. E. (2017). Data-driven event-by-event respiratory motion correction using TOF PET list-mode centroid of distribution, *Physics in Medicine and Biology* **62**(12): 4741–4755. Number: 12.
URL: *https://iopscience.iop.org/article/10.1088/1361-6560/aa700c*

Ren, S., Lu, Y., Bertolli, O., Thielemans, K. & Carson, R. E. (2019). Event-by-event non-rigid data-driven PET respiratory motion correction methods: comparison of principal component analysis and centroid of distribution, *Physics in Medicine & Biology* **64**(16): 165014. Number: 16.
URL: *https://iopscience.iop.org/article/10.1088/1361-6560/ab0bc9*

Rezaei, A., Defrise, M., Bal, G., Michel, C., Conti, M., Watson, C. & Nuyts, J. (2012). Simultaneous reconstruction of activity and attenuation in time-of-flight PET, *IEEE transactions on medical imaging* **31**(12): 2224–2233.

Rezaei, A., Defrise, M. & Nuyts, J. (2014). ML-Reconstruction for TOF-PET With Simultaneous Estimation of the Attenuation Factors, *IEEE Transactions on Medical Imaging* **33**(7): 1563–1572. Conference Name: IEEE Transactions on Medical Imaging.

Rezaei, A., Michel, C., Casey, M. E. & Nuyts, J. (2016). Simultaneous reconstruction of the activity image and registration of the CT image in TOF-PET, *Physics in Medicine & Biology* **61**(4): 1852.

Röhl, E., Schumacher, H. & Fischer, B. (2007). Automatic detection of abrupt patient motion in SPECT data acquisition, *in* K. R. Cleary, J. Hsieh, A. Manduca, J. P. W. Pluim, S. C. Horii, S. Y. Emelianov, M. L. Giger, Y. Jiang, B. Sahiner, N. Karssemeijer, S. A. McAleavey, K. P. Andriole, J. M. Reinhardt, X. P. Hu, M. J. Flynn & M. I. Miga (eds), *Proc. SPIE 6512, Medical Imaging 2007*, pp. 65120C–65120C–8. event-place: San Diego, CA, USA.
URL: *http://dx.doi.org/10.1117/12.708375*

Robson, P. M., Trivieri, M., Karakatsanis, N. A., Padilla, M., Abgral, R., Dweck, M. R., Kovacic, J. C. & Fayad, Z. A. (2018). Correction of respiratory and cardiac motion in cardiac PET/MR using MR-based motion modeling, *Physics in Medicine and Biology* **63**(22): 225011.

Rostampour, N., Jabbari, K., Esmaeili, M., Mohammadi, M. & Nabavi, S. (2018). Markerless Respiratory Tumor Motion Prediction Using an Adaptive Neuro-fuzzy Approach, *Journal of Medical Signals and Sensors* **8**(1): 25. Publisher: Wolters Kluwer – Medknow Publications.

URL: *https://www.ncbi.nlm.nih.gov/pmc/articles/PMC5840893/*

Schleyer, P., Hong, I., Jones, J., Hamill, J., Panin, V. & Fuerst, S. (2018). Data-Driven Respiratory Gating Whole Body PET Using Continuous Bed Motion, *2018 IEEE Nuclear Science Symposium and Medical Imaging Conference Proceedings (NSS/MIC)*, pp. 1–5. ISSN: 2577-0829.

Schleyer, P. J., O'Doherty, M. J., Barrington, S. F. & Marsden, P. K. (2009). Retrospective data-driven respiratory gating for PET/CT, *Physics in Medicine and Biology* **54**(7): 1935–1950.
URL: *http://dx.doi.org/10.1088/0031-9155/54/7/005*

Schleyer, P. J., O'Doherty, M. J. & Marsden, P. K. (2011). Extension of a data-driven gating technique to 3D, whole body PET studies., *Physics in medicine and biology* **56**(13): 3953–3965.
URL: *http://dx.doi.org/10.1088/0031-9155/56/13/013*

Schleyer, P. J., Thielemans, K. & Marsden, P. K. (2014). Extracting a respiratory signal from raw dynamic PET data that contain tracer kinetics, *Phys. Med. Biol.* **59**(15): 4345–4356.
URL: *http://stacks.iop.org/0031-9155/59/i=15/a=4345?key=crossref.622f7e791aee73f985440a9baa064d1d*

Schumacher, H., Modersitzki, J. & Fischer, B. (2009). Combined Reconstruction and Motion Correction in SPECT Imaging, *Nuclear Science, IEEE Transactions on* **56**(1): 73–80.
URL: *http://dx.doi.org/10.1109/tns.2008.2007907*

Sharp, J. T., Goldberg, N. B., Druz, W. S. & Danon, J. (1975). Relative contributions of rib cage and abdomen to breathing in normal subjects, *Journal of Applied Physiology* **39**(4): 608–618. Publisher: American Physiological Society.
URL: *https://journals.physiology.org/doi/abs/10.1152/jappl.1975.39.4.608*

Shepp, L. A. & Vardi, Y. (1982). Maximum likelihood reconstruction for emission tomography, *IEEE Transactions on Medical Imaging* **1**(2): 113–122.

Shi, L., Onofrey, J. A., Revilla, E. M., Toyonaga, T., Menard, D., Ankrah, J.-s., Carson, R. E., Liu, C. & Lu, Y. (2019). A Novel Loss Function Incorporating Imaging Acquisition Physics for PET Attenuation Map Generation using Deep Learning, *arXiv:1909.01394 [physics]* . arXiv: 1909.01394.
URL: *http://arxiv.org/abs/1909.01394*

Slart, R. H. J. A., Tsoumpas, C., Glaudemans, A. W. J. M., Noordzij, W., Willemsen, A. T. M., Borra, R. J. H., Dierckx, R. A. J. O. & Lammertsma, A. A. (2021). Long axial field of view PET scanners: a road map to implementation and new possibilities, *European Journal of Nuclear Medicine and Molecular Imaging* .
URL: *https://doi.org/10.1007/s00259-021-05461-6*

Slomka, P. J., Rubeaux, M., Le Meunier, L., Dey, D., Lazewatsky, J. L., Pan, T., Dweck, M. R., Newby, D. E., Germano, G. & Berman, D. S. (2015). Dual-Gated Motion-Frozen Cardiac PET with Flurpiridaz F 18, *Journal of Nuclear Medicine: Official Publication, Society of Nuclear Medicine* **56**(12): 1876–1881.

Stemkens, B., Tijssen, R., Denis De Senneville, B., Lagendijk, J. & Van Den Berg, C. (2016). Image-driven, model-based 3D abdominal motion estimation for MR-guided radiotherapy, *Physics in Medicine and Biology* **61**(14). Publisher: IOP Publishing.
URL: *https://hal.archives-ouvertes.fr/hal-01365987*

Sun, T. & Mok, G. S. (2012). Techniques for respiration-induced artifacts reductions in thoracic PET/CT, *Quantitative imaging in medicine and surgery* **2**(1): 46.

Tenenbaum, J. B., de Silva, V. & Langford, J. C. (2000). A Global Geometric Framework for Nonlinear Dimensionality Reduction, *Science* **290**(5500): 2319–2323.
URL: *http://dx.doi.org/10.1126/science.290.5500.2319*

Thielemans, K. (2005). Scatter Estimation and Motion Correction in PET, *IEEE Nuclear Science Symposium Conference Record, 2005*, Vol. 3, IEEE, pp. 1745–1747. event-place: Wyndham El Conquistador Resort, Puerto Rico.
URL: *http://dx.doi.org/10.1109/nssmic.2005.1596657*

Thielemans, K., Gopalakrishnan, G., Roy, A., Srikrishnan, V., Thiruvenkadam, S., Wollenweber, S. D. & Manjeshwar, R. M. (2011). Robust motion correction for respiratory gated PET/CT using

weighted averaging, *2011 IEEE Nuclear Science Symposium Conference Record*, pp. 2964–2967. ISSN: 1082-3654.

Thielemans, K., Rathore, S., Engbrant, F. & Razifar, P. (2011). Device-less gating for PET/CT using PCA, *2011 IEEE Nuclear Science Symposium and Medical Imaging Conference (2011 NSS/MIC)*, IEEE, pp. 3904–3910. tex.ids: thielemans2011DevicelessGatingPETa ISSN: 1082-3654 event-place: Valencia, Spain.
URL: *http://dx.doi.org/10.1109/nssmic.2011.6153742*

Thielemans, K., Schleyer, P., Marsden, P. K., Manjeshwar, R. M., Wollenweber, S. D. & Ganin, A. (2013). Comparison of different methods for data-driven respiratory gating of PET data, *Nuclear Science Symposium and Medical Imaging Conference (NSS/MIC), 2013 IEEE*, IEEE, pp. 1–4. event-place: Seoul, Korea.
URL: *http://dx.doi.org/10.1109/nssmic.2013.6829055*

Thiruvenkadam, S., Shriram, K., Manjeshwar, R. & Wollenweber, S. (2015). Robust PET Motion Correction Using Non-local Spatio-temporal Priors, *in* N. Navab, J. Hornegger, W. M. Wells & A. Frangi (eds), *Medical Image Computing and Computer-Assisted Intervention – MICCAI 2015*, Lecture Notes in Computer Science, Springer International Publishing, Cham, pp. 643–650.

Thorndyke, B., Schreibmann, E., Koong, A. & Xing, L. (2006). Reducing respiratory motion artifacts in positron emission tomography through retrospective stacking, *Medical Physics* **33**(7): 2632+.
URL: *http://dx.doi.org/10.1118/1.2207367*

Törnqvist, E., Månsson, A., Larsson, E. M. & Hallström, I. (2006). Impact of extended written information on patient anxiety and image motion artifacts during magnetic resonance imaging, *Acta Radiologica (Stockholm, Sweden: 1987)* **47**(5): 474–480.

Tsoumpas, C., Mackewn, J. E., Halsted, P., King, A. P., Buerger, C., Totman, J. J., Schaeffter, T. & Marsden, P. K. (2010). Simultaneous PET–MR acquisition and MR-derived motion fields for correction of non-rigid motion in PET, *Annals of nuclear medicine* **24**(10): 745–750.

Tsoumpas, C., Polycarpou, I., Thielemans, K., Buerger, C., King, A. P., Schaeffter, T. & Marsden, P. K. (2013). The effect of regularization in motion compensated PET image reconstruction: a realistic numerical 4D simulation study., *Physics in medicine and biology* **58**(6): 1759–1773.
URL: *http://dx.doi.org/10.1088/0031-9155/58/6/1759*

van den Hoff, J., Maus, J. & Schramm, G. (2020). Motion compensation in emission tomography, *Handbook of Particle Detection and Imaging*, Springer International Publishing, pp. 1–47.

Van der Maaten, L. J. P., Postma, E. O. & Van Den Herik, H. J. (2009). Dimensionality reduction: A comparative review, *Journal of Machine Learning Research* **10**.

van Elmpt, W., Hamill, J., Jones, J., De Ruysscher, D., Lambin, P. & Ollers, M. (2011). Optimal gating compared to 3D and 4D PET reconstruction for characterization of lung tumours, *European Journal of Nuclear Medicine and Molecular Imaging* **38**(5): 843–855.

Visvikis, D., Barret, O., Fryer, T., Turzo, A., Lamare, F., Le Rest, C. & Bizais, Y. (2003). A posteriori respiratory motion gating of dynamic PET images, *Nuclear Science Symposium Conference Record, 2003 IEEE* **5**: 3276–3280 Vol.5.
URL: *http://dx.doi.org/10.1109/nssmic.2003.1352596*

Visvikis, D., Lamare, F., Bruyant, P., Boussion, N. & Cheze Le Rest, C. (2006). Respiratory motion in positron emission tomography for oncology applications: Problems and solutions, *Nuclear Instruments and Methods in Physics Research Section A: Accelerators, Spectrometers, Detectors and Associated Equipment* **569**(2): 453–457.
URL: *http://www.sciencedirect.com/science/article/pii/S0168900206015014*

Wachinger, C., Yigitsoy, M., Rijkhorst, E.-J. & Navab, N. (2011). Manifold learning for image-based breathing gating in ultrasound and MRI, *Medical Image Analysis* .
URL: *http://dx.doi.org/10.1016/j.media.2011.11.008*

Walker, M. D., Morgan, A. J., Bradley, K. M. & McGowan, D. R. (2019). Evaluation of data-driven respiratory gating waveforms for clinical PET imaging, *EJNMMI Res* **9**(1): 1.

Wallach, D., Lamare, F., Kontaxakis, G. & Visvikis, D. (2012). Super-Resolution in Respiratory Synchronized Positron Emission Tomography, *IEEE Transactions on Medical Imaging* **31**(2): 438–448. Conference Name: IEEE Transactions on Medical Imaging.

Wang, G., Rahmim, A. & Gunn, R. N. (2020). PET Parametric Imaging: Past, Present, and Future, *IEEE Transactions on Radiation and Plasma Medical Sciences* **4**(6): 663–675. Conference Name: IEEE Transactions on Radiation and Plasma Medical Sciences.

Wentz, T., Fayad, H., Bert, J., Pradier, O., Clément, J.-F., Vourch, S., Boussion, N. & Visvikis, D. (2012). Accuracy of dynamic patient surface monitoring using a time-of-flight camera and B-spline modeling for respiratory motion characterization, *Physics in Medicine and Biology* **57**(13): 4175–4193. Publisher: IOP Publishing.
URL: *https://hal.archives-ouvertes.fr/hal-00948363*

Whitehead, A. C., Biguri, A., Efthimiou, N., Su, K.-H., Wollenweber, S. W., Stearns, C. W., Hutton, B. F., McClelland, J. R. & Thielemans, K. (2020). PET/CT Respiratory Motion Correction With a Single Attenuation Map Using NAC Derived Deformation Fields, *2020 IEEE Nuclear Science Symposium and Medical Imaging Conference (NSS/MIC)*, pp. 1–3. ISSN: 2577-0829.

Wilms, M., Werner, R., Yamamoto, T., Handels, H. & Ehrhardt, J. (2017). Subpopulation-based correspondence modelling for improved respiratory motion estimation in the presence of inter-fraction motion variations, *Physics in Medicine and Biology* **62**: 5823.
URL: *http://adsabs.harvard.edu/abs/2017PMB....62.5823W*

Wollenweber, S. D., Gopalakrishnan, G., Thielemans, K. & Manjeshwar, R. M. (2012). Evaluation of the Accuracy and Robustness of a Motion Correction Algorithm for PET Using a Novel Phantom Approach, *Nuclear Science, IEEE Transactions on* **59**(1): 123–130.
URL: *http://dx.doi.org/10.1109/tns.2011.2179983*

Wolthaus, J. W. H., van Herk, M., Muller, S. H., Belderbos, J. S. A., Lebesque, J. V., de Bois, J. A., Rossi, M. M. G. & Damen, E. M. F. (2005). Fusion of respiration-correlated PET and CT scans: correlated lung tumour motion in anatomical and functional scans, *Physics in Medicine and Biology* **50**(7): 1569–1583.

Würslin, C., Schmidt, H., Martirosian, P., Brendle, C., Boss, A., Schwenzer, N. F. & Stegger, L. (2013). Respiratory motion correction in oncologic PET using T1-weighted MR imaging on a simultaneous whole-body PET/MR system, *Journal of nuclear medicine* **54**(3): 464–471.

Yu, Y., Chan, C., Ma, T., Liu, Y., Gallezot, J.-D., Naganawa, M., Kelada, O. J., Germino, M., Sinusas, A. J., Carson, R. E. & Liu, C. (2016). Event-by-Event Continuous Respiratory Motion Correction for Dynamic PET Imaging, *Journal of Nuclear Medicine* **57**(7): 1084–1090. Number: 7.
URL: *http://jnm.snmjournals.org/cgi/doi/10.2967/jnumed.115.167676*

Zhang, Q., Souvenir, R. & Pless, R. (2006). On Manifold Structure of Cardiac MRI Data: Application to Segmentation, *Computer Vision and Pattern Recognition, 2006 IEEE Computer Society Conference on*, Vol. 1, IEEE, pp. 1092–1098. event-place: New York, NY, USA.
URL: *http://dx.doi.org/10.1109/cvpr.2006.214*

Zhang, Y., Yang, J., Zhang, L., Court, L. E., Balter, P. A. & Dong, L. (2013). Modeling respiratory motion for reducing motion artifacts in 4D CT images, *Medical Physics* **40**(4): 041716. _eprint: https://aapm.onlinelibrary.wiley.com/doi/pdf/10.1118/1.4795133.
URL: *https://aapm.onlinelibrary.wiley.com/doi/abs/10.1118/1.4795133*